U.S. DEPARTMENT OF THE INTERIOR
U.S. GEOLOGICAL SURVEY

Prepared for the
NATIONAL AERONAUTICS AND SPACE ADMINISTRATION

GEOLOGIC INVESTIGATIONS SERIES I–2721
ATLAS OF VENUS: PANDROSOS DORSA QUADRANGLE (V–5)

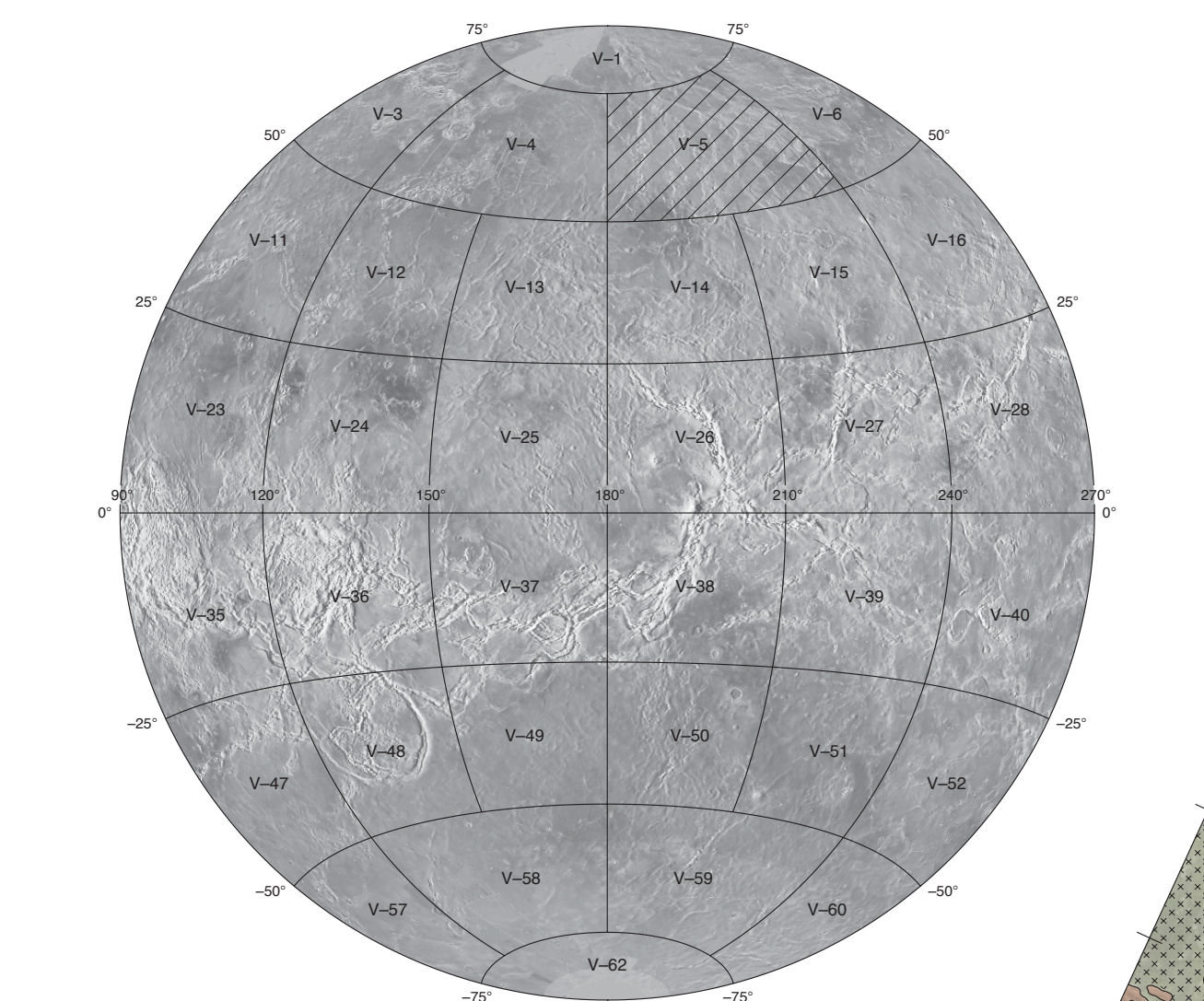

QUADRANGLE LOCATION
Photomosaic showing location of map area. An outline of 1:5,000,000-scale quadrangles is provided for reference.

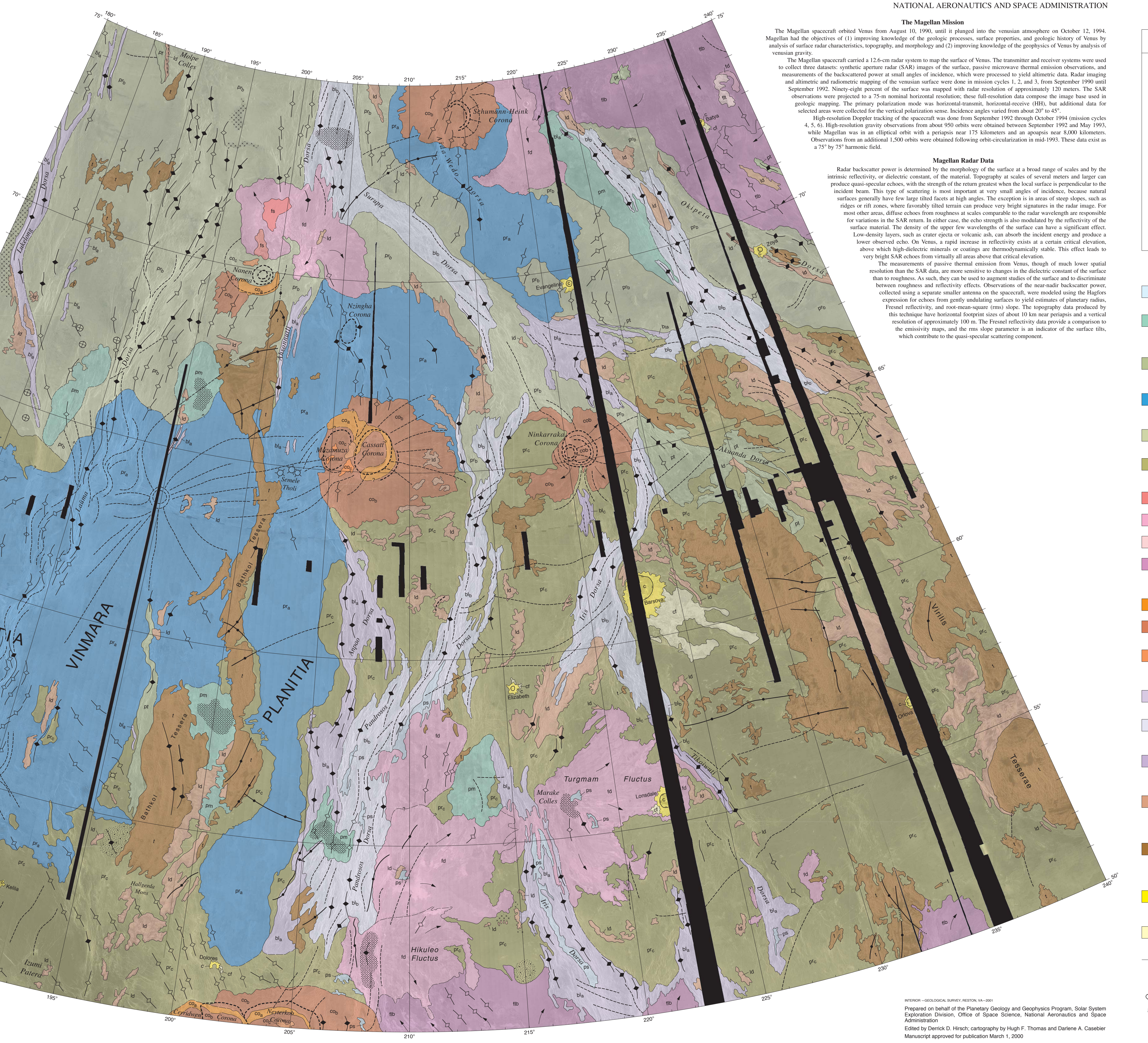

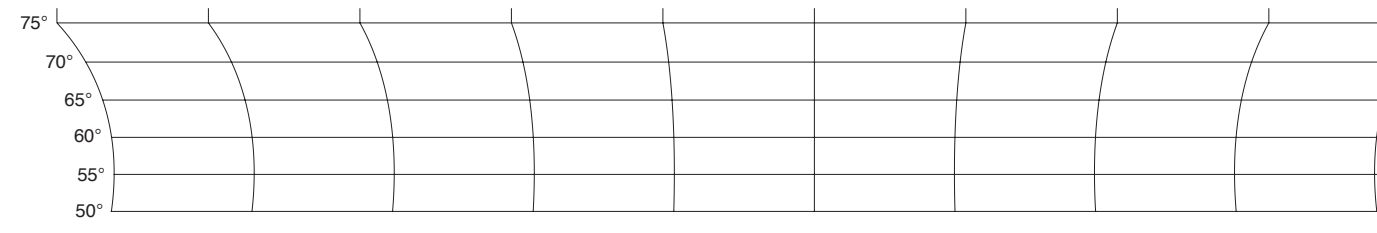

SCALE 1:4 711 886 (1 mm = 4.712 km) AT 25° LATITUDE
1:5 000 000 AT 34° and 73° LATITUDES
LAMBERT PROJECTION

INTERIOR—GEOLOGICAL SURVEY, RESTON, VA—2001
Prepared on behalf of the Planetary Geology and Geophysics Program, Solar System Exploration Division, Office of Space Science, National Aeronautics and Space Administration
Edited by Derrick D. Hirsch; cartography by Hugh F. Thomas and Darlene A. Casebier
Manuscript approved for publication March 1, 2000

The Magellan Mission

The Magellan spacecraft orbited Venus from August 10, 1990, until it plunged into the venusian atmosphere on October 12, 1994. Magellan had the objectives of (1) improving knowledge of the geologic processes, surface properties, and geologic history of Venus by analysis of surface radar characteristics, topography, and morphology and (2) improving knowledge of the geophysics of Venus by analysis of venusian gravity.

The Magellan spacecraft carried a 12.6-cm radar system to map the surface of Venus. The transmitter and receiver systems were used to collect three datasets: synthetic aperture radar (SAR) images of the surface, passive microwave thermal emission observations, and measurements of the backscattered power at small angles of incidence, which were processed to yield altimetric data. Radar imaging and altimetric and radiometric mapping of the venusian surface were done in mission cycles 1, 2, and 3, from September 1990 until September 1992. Ninety-eight percent of the surface was mapped with radar resolution of approximately 120 meters. The SAR observations were projected to a 75-m nominal horizontal resolution; these full-resolution data compose the image base used in geologic mapping. The primary polarization mode was horizontal-transmit, horizontal-receive (HH), but additional data for selected areas were collected for the vertical polarization sense. Incidence angles varied from about 20° to 45°.

High-resolution Doppler tracking of the spacecraft was done from September 1992 through October 1994 (mission cycles 4, 5, 6). High-resolution gravity observations from about 950 orbits were obtained between September 1992 and May 1993, while Magellan was in an elliptical orbit with a periapsis near 175 kilometers and an apoapsis near 8,000 kilometers. Observations from an additional 1,500 orbits were obtained following orbit-circularization in mid-1993. These data exist as a 75° by 75° harmonic field.

Magellan Radar Data

Radar backscatter power is determined by the morphology of the surface at a broad range of scales and by the intrinsic reflectivity, or dielectric constant, of the material. Topography at scales of several meters and larger can produce quasi-specular echoes, with the strength of the return greatest when the local surface is perpendicular to the incident beam. This type of scattering is most important at very small angles of incidence, because natural surfaces generally have few large tilted facets at high angles. The exception is in areas of steep slopes, such as ridges or rift zones, where favorably tilted terrain can produce very bright signatures in the radar image. For most other areas, diffuse echoes from roughness at scales comparable to the radar wavelength are responsible for variations in the SAR return. In either case, the echo strength is also modulated by the reflectivity of the surface material. The density of the upper few wavelengths of the surface can have a significant effect. Low-density layers, such as crater ejecta or volcanic ash, can absorb the incident energy and produce a lower observed echo. On Venus, a rapid increase in reflectivity exists at a certain critical elevation, above which high-dielectric minerals or coatings are thermodynamically stable. This effect leads to very bright SAR echoes from virtually all areas above that critical elevation.

The measurements of passive thermal emission from Venus, though of much lower spatial resolution than the SAR data, are more sensitive to changes in the dielectric constant of the surface than to roughness. As such, they can be used to augment studies of the surface and to discriminate between roughness and reflectivity effects. Observations of the near-nadir backscatter power, collected using a separate smaller antenna on the spacecraft, were modeled using the Hagfors expression for echoes from gently undulating surfaces to yield estimates of planetary radius, Fresnel reflectivity, and root-mean-square (rms) slope. The topography data produced by this technique have horizontal footprint sizes of about 10 km near periapsis and a vertical resolution of approximately 100 m. The Fresnel reflectivity data provide a comparison to the emissivity maps, and the rms slope parameter is an indicator of the surface tilts, which contribute to the quasi-specular scattering component.

CORRELATION OF MAP UNITS

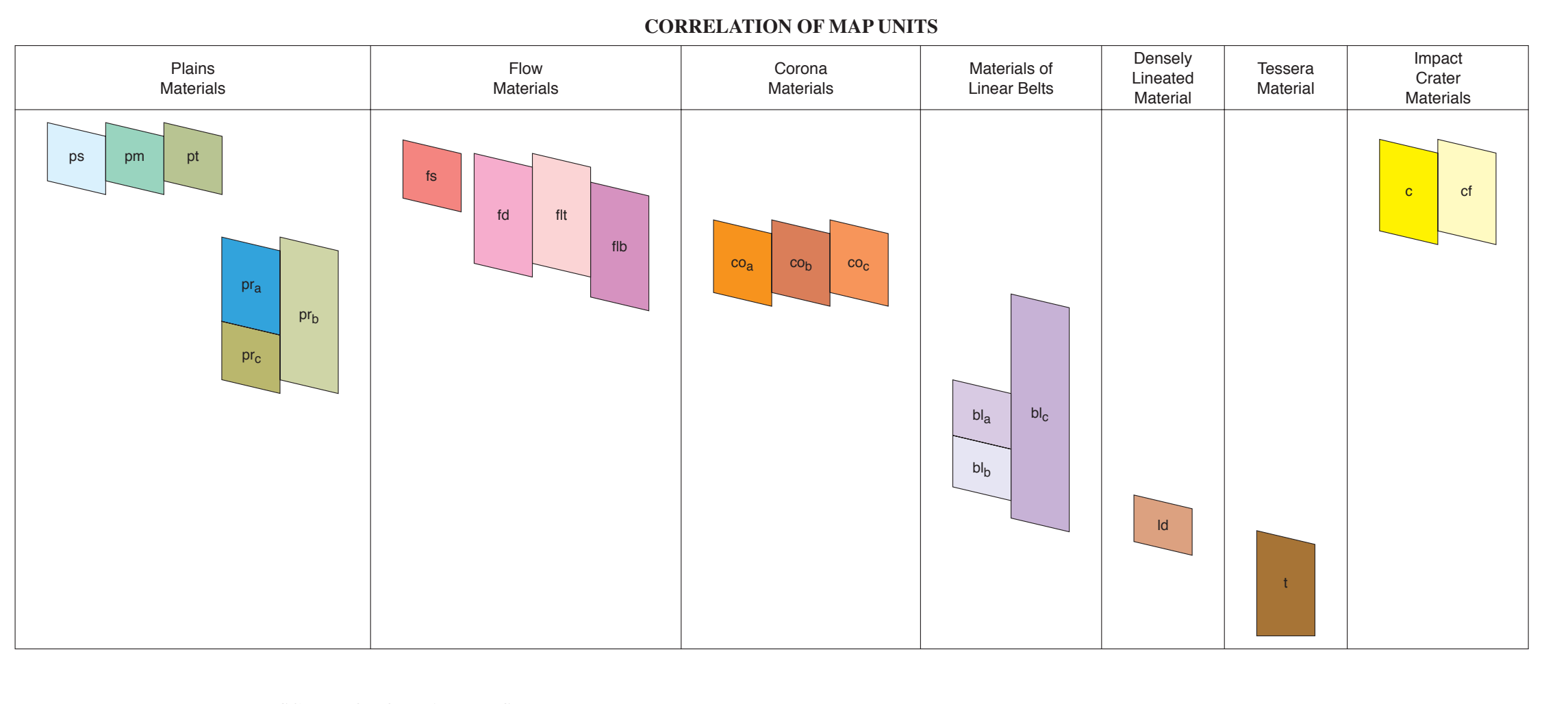

DESCRIPTION OF MAP UNITS

PLAINS MATERIALS

ps **Smooth local plains material**—Homogeneous radar-dark plains material having intermediate radar backscatter coefficient (–11.499). Contains few to no radar-bright linear features. Locally embays tessera material and deformation belt topographic rises. Occurs as small outliers within zones of high deformation. *Interpretation*: Young volcanic material

pm **Mottled local plains material**—Locally distributed plains material characterized by small-scale (20 km) blotchy pattern of moderately bright to moderately dark patches having intermediate radar backscatter coefficient (–11.715). Mottled appearance commonly associated with small-scale shields. Contains few to no radar-bright linear features. Appears to be superposed upon regional plains materials, although contacts are commonly gradational. *Interpretation*: Concentrations of small shield volcanoes and flank flows

pt **Textured local plains material**—Moderately radar-bright to radar-bright material with a generally diffuse, grainy, or textured appearance and high radar backscatter coefficient (–8.205). Commonly occurs as small patches tens of kilometers across within highly deformed regions. Embays regional plains materials. *Interpretation*: Outliers of rough material; radar brightness possibly caused by extremely dense fractures finer than resolution

pr_a **Radar-bright regional plains material**—Broadly distributed material having intermediate radar backscatter coefficient (–11.61) that is lower than average scattering law for Venus but high with respect to other regional plains units. Mostly homogeneous although locally blotchy with materials of slightly less brightness. Some wrinkle ridges visible at highest resolution. Locally infills fractures within unit prc. *Interpretation*: Lava flows

pr_b **Intermediate regional plains material**—Broadly distributed radar-dark to radar-bright variegated plains material with an overall diffuse appearance. Radar backscatter coefficient between that of units pr_c and pr_a (–12.06). Contacts are commonly gradational. *Interpretation*: Lava flows with superposed aeolian features

pr_c **Radar-dark regional plains material**—Broadly distributed material having low radar backscatter coefficient (–13.61). Locally embays tessera material and infills grabens. Locally contains high concentration of radar-bright fractures. *Interpretation*: Lava flows

FLOW MATERIALS

fs **Slump material**—Radar-bright to radar-dark material that contains an abundance of curvilinear radar-bright linear features. Has high radar backscatter coefficient (–7.24). *Interpretation*: Slump material

fd **Digitate flow material**—Material of radar-bright to radar-dark digitate flow fields having radar backscatter coefficient ranging from –10.13 to –7.89. Commonly associated with regions of highly concentrated shield volcanoes. *Interpretation*: Lava flows; probably basaltic

flt **Lineated flow material**—Radar-bright material having intersecting sets of fractures with very high radar backscatter coefficient (–5.53). *Interpretation*: Relatively old volcanic flow with subsequent deformation

flb **Lobate flow material**—Material of radar-bright and radar-dark lobate flow fields with a range of radar backscatter coefficients from –12.28 to –6.97. Contains a few digitate flows. *Interpretation*: Flow materials related to montes and coronae outside of quadrangle boundaries; probably basaltic

CORONA MATERIALS

co_a **Corona material a**—Radar-bright material within concentric linear features around corona structures; high radar backscatter coefficient (–9.47) and homogeneous texture. Superposed on some corona structures. *Interpretation*: Volcanic deposit associated with corona development

co_b **Corona material b**—Intermediate to radar-dark flow material areally associated with corona structures; intermediate radar backscatter coefficient (–11.80). Occurs as both digitate and lobate patterns. Superposed on regional plains materials. *Interpretation*: Lava flows associated with corona development

co_c **Corona material c**—Radar bright material with intersecting sets of fractures similar to tessera terrain; high radar backscatter coefficient (–6.76). Superposed on all surrounding materials. *Interpretation*: Flows associated with corona development that either become deformed with corona evolution or have intrinsically rougher surfaces than surrounding materials

MATERIALS OF LINEAR BELTS

bl_a **Linear belt material a**—Moderately radar-bright material associated with linear belts. Has an intermediate radar backscatter coefficient (–9.971). Contains ridges and sparse radar-bright linear features. Embayed by surrounding plains materials. Most contacts are distinct, a few are either gradational or ambiguous. *Interpretation*: Deformed material of uncertain origin

bl_b **Linear belt material b**—Radar-bright to radar-dark material associated with linear belts. Has a high radar backscatter coefficient (–7.05). Contains ridges and a penetrative and dense pattern of linear features. Linear features more abundant than in unit bl_a. The densely spaced linears cross the ridges and are present in most of the material between individual ridges. *Interpretation*: Deformed material of uncertain origin

bl_c **Linear belt material c**—Material containing pronounced topography, radar-bright linears, ridges, and lobate margins. Radar backscatter coefficient due predominantly to structural deformation. *Interpretation*: Deformed material of uncertain origin, but may include deformed regional or local plains materials

DENSELY LINEATED MATERIAL

ld **Densely lineated material**—Radar-bright to radar-intermediate material having a radar backscatter coefficient of –9.208. Commonly occurs within topographic high tessera blocks and linear belts. Contains abundant densely spaced, parallel linear features. Embays tessera material. Also occurs as small patches, commonly with wispy edges, embayed by surrounding plains materials. *Interpretation*: Deformed plains? material older than regional plains materials

TESSERA MATERIAL

t **Tessera material**—Radar-bright material having high radar backscatter coefficient (–7.507). Contains at least two sets of fractures, ridges, and grabens that intersect at high angles. Material and all structures are embayed and truncated by all surrounding materials. Present as large blocks parallel to north-south-trending linear belts and as scattered small inliers. *Interpretation*: Old, highly deformed material of unknown origin

IMPACT CRATER MATERIALS

c **Crater material, undifferentiated**—Radar-bright material having a high radar backscatter coefficient (–7.20). Includes floor, rim, ejecta, and central peak materials. Hummocky texture. Superposed on all surrounding materials. Some floor materials are radar-dark (for example, Barsova crater). *Interpretation*: Deposits and structures caused by bolide impact; radar-dark floor material either ponded impact melt or younger lava

cf **Crater flow material**—Radar-bright to radar-dark, mottled flow material associated with impact craters. Intermediate radar backscatter coefficient (–11.56). *Interpretation*: Melt generated by bolide impact event; lavalike flow deposit

Contact—Dashed where approximate; dotted where buried; queried where uncertain

Impact crater rim—5–20 km diameter

Impact crater rim—≥20 km diameter

Depression

Corona annulus

Flat-topped volcanic dome—Diameter ≥10 km

Volcanic shield with flow

Flow direction

Shield field

Aeolian feature

Ridge

Wrinkle ridge

Lineament

Graben—Dotted where buried

Channel—Dotted where buried

Splotch feature

INTRODUCTION

The Pandrosos Dorsa quadrangle (V–5), Venus, lies between latitudes 50° N. and 75° N. and longitudes 180° E. and 240° E. and includes the northern part of Vinmara Planitia. The quadrangle encompasses approximately 10 million square kilometers of the northern low-lying plains of the venusian surface and sits at an average radius of 6051.30 kilometers, approximately 500 meters below the mean planetary radius of 6051.84 kilometers.

Vinmara Planitia is dominated by a highly complex pattern of long, narrow, apparently deformed belts and their surrounding regional plains. These belts are defined as large-scale linear zones that contain and confine smaller scale ridges and radar-bright linear features; they are termed "linear belts" in this report. Vinmara Planitia contains one of the two highest concentrations of linear belts on Venus; the second being within Lavinia Planitia in the southern hemisphere. Unlike the belts of Lavinia Planitia, the linear belts of Vinmara Planitia contain a wide variety of morphologic styles, and the material within these belts spans a significant age range. Furthermore, the belts within Vinmara Planitia cover a surface area three times greater than the belts in Lavinia Planitia.

All or parts of twelve linear belts are within the Pandrosos Dorsa quadrangle: Lukelong, Laūma, Okipeta, Iris, Surupa, Ahsonnuti, Akuanda, Tikoiwati, Aida-Wedo, Anpao (the linear belt in the longitudinal center of the quadrangle), an unnamed belt, and Pandrosos, the linear belt for which the quadrangle is named. Other small concentrations of ridges are present but are not substantial enough to be cataloged as major linear belts. Topographically, the belts commonly reach heights of approximately one kilometer above the surrounding plains, although portions of the belts are not elevated or even occur within troughs. Together, the twelve linear belts create a fanlike geometric pattern in plan view and form the majority of what has been referred to as the "Ridge Belt Plains-Fan Assemblage" (Frank and Head, 1990). As this name implies, some of the features within the belts are ridges. However, nearly half of the features within the belt boundaries are either recognizable grabens or radar-bright linear features, which are generally interpreted as extensional fractures. Therefore, the more general term "linear belt" is preferable to ridge belt. The linear belts of the Pandrosos Dorsa quadrangle continue northward to the pole and southward into the regions of Nemesis Tessera (V–14) and Bellona Fossae (V–15) where they lose their intensity and eventually die out (Zimbelman, 1995).

In addition to the linear belts, the quadrangle includes the easternmost part of the regional plains of Atalanta Planitia and the northern part of Vinmara Planitia. These widespread plains lie approximately 500 meters below the mean planetary radius and show little to no topography. Atalanta and Vinmara Planitiae are similar to other regional plains covering nearly 80% of the global surface (Masursky and others, 1980), except that the plains of Vinmara contain far fewer wrinkle ridges.

The quadrangle also includes two large and elongate patches of tessera: Virilis on the east edge of the quadrangle and Bathkol farther west. These blocks of tessera materials mimic the nearly north-south orientation of the linear belts at elevations approximately one kilometer above the surrounding regional plains. Other major features within the quadrangle include twelve impact craters, two of which are large and include outflow material; nine coronae and coronalike features; seven volcanic shield fields; numerous small tessera inliers; and part of one lava channel.

This region is of geologic interest because it contains the most widespread and largest concentration of extensive linear belts on Venus, and thus it is an ideal area to study the temporal and genetic relations between linear belts and regional plains. The variety of morphologies, structural styles, and temporal relations within the Pandrosos Dorsa quadrangle provides a unique opportunity for establishing stratigraphic relations not only among material units but also among tectonic episodes. Because the preserved record of tectonic processes on Venus is different from that of the oceanic plate tectonics we recognize on Earth (Solomon and others, 1991, 1992), the Pandrosos Dorsa quadrangle is a key region of study for illuminating past and present tectonic styles of Venus. Interpretations extracted from this study may apply to other venusian linear belts and may help explain crustal and upper mantle properties and processes.

METHODS AND DATA USED

The accompanying 1:5 million-scale geologic map was prepared using Magellan radar imagery at several resolutions. The base map is a controlled mosaic of Magellan Synthetic Aperture Radar (SAR) data prepared by the U.S. Geological Survey. The data were collected during the cycle 1 imaging with a west-to-east look direction. Initial mapping was based on Compressed Once Mosaicked Image Data Records (C1-MIDR's) having a resolution of 225 meters/pixel. A more detailed, higher resolution analysis was completed using digital Full Resolution Mosaicked Image Data Records (F-MIDR's) and F-maps (hard copies of 12° by 18°, 12° by 24°, and 12° by 36° regions at full resolution) which have an oversampled resolution of 75 meters/pixel. Altimetry, emissivity, root mean square slope, and Fresnel reflectivity also provided useful mapping information, especially with respect to delineating volcanic flows and surficial deposits. Synthetic parallax stereo images also were utilized.

SAR incidence angles within the Pandrosos Dorsa quadrangle range from 33° at 50° latitude to 23° at 75° latitude. Below an incidence angle of about 25°, smoother surfaces have greater backscatter than rougher surfaces (Farr, 1993). A moderately rough surface, with wavelength approximating the 12.6 cm wavelength of the radar beam, has backscatter of –12 dB at 23° and –20 dB at 33°, the incidence-angle range within the Pandrosos Dorsa quadrangle. In general, and independent of wavelength, surfaces appear smoother as incidence angles increase; therefore, materials toward the southern part of the quadrangle appear smoother than similar materials in the northern part of the quadrangle. This difference in appearance may lead to erroneous interpretation of material units if incidence angles are not taken into account when mapping.

Stratigraphic material units were defined primarily on the basis of relative radar brightness, fabrics, and cross-cutting and superposition relations as displayed in the cycle 1 SAR images. Ancillary radar properties (radar backscatter coefficient, emissivity, Fresnel reflectivity, and root mean square slope) were calculated using programs provided by Campbell (1995). Further explanation of Magellan data collection and general methodology for SAR analysis can be found in Ford and others (1989).

STRATIGRAPHY

The stratigraphic units within the boundaries of the Pandrosos Dorsa quadrangle are categorized according to type location and material characteristics. Twenty units are defined: one tessera unit, one densely lineated unit, three materials confined to linear belts, six plains units, four flow units, three corona units, and two impact crater units. Units are defined primarily according to their relative radar brightness on the SAR image, homogeneity of the radar brightness, and texture. Other defining factors are cross-cutting relations and truncation of structures and fabrics. Whereas crater densities are useful in determining relative ages among underlying units on other planets, the small number of craters on Venus and their globally random distribution (Schaber and others, 1992; Strom and others, 1994) make this dating tool essentially useless for mapping at this scale.

TESSERA MATERIAL

The oldest material unit present within the Pandrosos Dorsa quadrangle is comparable in appearance to that described from Venera images as tessera by Basilevsky and others (1986). Tessera material (unit t) is characterized by its bright backscatter coefficient (averaging –7.507 dB) and high density of closely spaced linear features, which have at least two orientations at high angles to each other. The bright backscatter is inferred to result from high surface roughness at centimeter scale combined with the abundance of linear features, most of which are inferred to be fractures. Two distinctly different sizes of tessera exposures occur in the Pandrosos Dorsa quadrangle: two large blocks, Virilis and Bathkol Tesserae, are thousands of kilometers long, whereas the abundant small patches are tens of kilometers across. Virilis Tessera is on the east edge of the quadrangle and has no distinct trend. Bathkol Tessera is centered at 198.0° E. longitude and has a general north-south trend that mimics that of the linear belts. Each of these large blocks of tessera spans approximately 20° in latitude. The dozens of smaller patches of tessera material are widely distributed throughout the quadrangle.

Both the large blocks and the small patches are inferred to be inliers, poking through the surrounding plains material from beneath. Commonly, tessera material is cut by grabens as much as 8 kilometers wide, which generally are filled by the surrounding plains material. The materials in contact with tessera material consistently truncate all of the linear features present within the tessera, supporting the inference that tessera consists of the oldest material within Vinmara Planitia.

DENSELY LINEATED MATERIAL

Densely lineated material (unit ld) occurs within linear belts, at the edges of large blocks of tessera, and as small scattered inliers within the regional plains materials. Unit ld is characterized by moderate radar backscatter (–9.208 dB), which appears to result from a unidirectional linear fabric having a characteristic spacing of tens of meters. The dominant trend of this fabric in the quadrangle is northwest-southeast, but locally it is northeast southwest, implying some regional variation in principal stress orientation. Densely lineated material is consistently embayed by all material units with the exception of tessera, making it the second oldest unit in the quadrangle.

MATERIALS OF THE LINEAR BELTS

Although numerous material units are located within the linear belts, only three materials are exclusive to the belts: linear belt materials a, b, and c, hereafter referred to as belt materials a, b, and c. The origins of these materials are unknown.

Belt material c (unit bl_c) is characterized by bright radar backscatter and high density of structural features such as ridges and radar-bright linear features. Unlike belt materials a and b, belt material c lacks undeformed portions that might provide information for stratigraphic correlation. Two relatively small regions of belt material c are mapped; they represent approximately five percent of the area covered by materials of the linear belts. A backscatter coefficient has not been measured for belt material c because it would reflect only the radar brightness due to structural and topographic features. The material is possibly a correlative of belt material a or b, but topographic and structural masking prevents unambiguous correlation.

Belt material b (unit bl_b) is characterized by a relatively bright backscatter coefficient (–7.050 dB), which indicates the surface is slightly rougher at centimeter scale than that of belt material a. As with belt material a, belt material b contains ridges that follow the trend of the belt itself, but the trend of the dense and pervasive radar-bright linear features varies from subparallel to approximately 30° from the trend of the belt. Belt material b is embayed by all surrounding material units with the exception of tessera material and densely lineated material. Most of the linear belts in the study region are composed exclusively of belt material b.

Belt material b is inferred to be older than belt material a from the single region within the Pandrosos Dorsa quadrangle in which the two units are in direct contact (near 55°–58° N., 206.2°E.). The relative ages are based primarily on cross-cutting relations and topography (see Structural Geology section).

Belt material a (unit bl_a) has moderately bright backscatter (–9.971 dB) and contains ridges and narrow radar-bright linear features. The trend of the ridges within belt material a generally parallels the trend of the belt itself, but the few radar-bright linear features within the material are consistently oriented approximately 50° to the trend of the ridges. Belt material a is embayed by all surrounding regional plains materials.

PLAINS MATERIALS

The Pandrosos Dorsa quadrangle contains three regionally widespread plains units and three local plains units. The regional plains materials are defined by their spatial extensiveness and relative brightness on SAR images. Each regional plains unit has characteristic homogeneity in radar brightness and is interpreted to be the result of extensive flooding by basaltic materials. As indicated by their 1.5°–3.0° root mean square slopes (table 1), the regional plains materials are relatively smooth at hundred meter scale. At centimeter scale, however, they differ in roughness (fig. 1; table 1). From smoothest to roughest, the regional plains have been defined as radar dark (unit pr_c); intermediate (unit pr_b); and bright (unit pr_a).

The radar-dark regional plains material covers approximately 20% of the quadrangle's surface area. Radar-dark regional plains material (unit pr_c) is characterized by a homogeneous, relatively low backscatter coefficient and a 2.32° root mean square slope, which are indicative of a smooth surface at both centimeter and hundred meter scales (fig. 1; table 1). The backscatter coefficients of the radar-dark regional plains plot between terrestrial very smooth ponded lava flows and pahoehoe flows (fig. 1). Locally, radar-dark regional plains material embays tessera material and fills grabens that cut the tessera, and it also embays and truncates structures within densely lineated plains, indicating that the radar-dark regional plains material is younger than both. Where radar-dark plains material is in contact with linear belts, the plains material is younger than both the linear features and the materials within the belt.

The scarcity of wrinkle ridges in the radar-dark plains material is puzzling. All other characteristics of radar-dark regional plains material suggest that it is related to the global plains inferred to have formed by extensive resurfacing approximately 300 million years ago (Strom and others, 1994), and most of the regional plains inferred to be the result of this resurfacing are characterized by common to abundant wrinkle ridges (for example, Squyres and others, 1992; Basilevsky and Head, 1995).

The absence of clear embayment relations (for example, indistinct unit boundaries) prevents determining a relative stratigraphic age for intermediate regional plains material (unit pr_b). The irregular and indistinct nature of many contacts suggests subsequent aeolian reworking of materials. Therefore, the difference in radar backscatter as seen on the SAR image alone distinguishes this unit from the other regional plains units.

Radar-bright regional plains material (unit pr_a) covers roughly 40% of the surface area of the Pandrosos Dorsa quadrangle. Most of the radar-bright regional plains are concentrated in the western half of the quadrangle, from approximately 85° E. to 205° E. Although the radar bright regional plains material is characterized as bright, the backscatter coefficients plot between very smooth ponded lava flows and pahoehoe flows as measured on Earth (fig. 1). Regardless of the local splotchy patterns within lobate flow forms, the sampled portions of radar-bright regional plains material follow the general trend of the Muhleman curve (fig. 1). This trend indicates that these plains have the consistent homogeneous properties characteristic of regional plains materials on Venus.

Radar-bright regional plains material consistently fills narrow grabens within the radar-dark regional plains and embays Bathkol Tessera and parts of Pandrosos Dorsa, indicating that it is younger. However, in some places along Laūma Dorsa the radar-bright regional plains material appears to be deformed into short-wavelength ridges and wrinkle ridges which, along with the absence of embayment relations in Laūma Dorsa, implies that emplacement of the radar-bright regional plains predates the latest deformational episode associated with Laūma Dorsa.

A few structural features are present within the three regional plains units, including a small number of east-west trending long linear features, grabens, and some wrinkle ridges. Wrinkle ridges are subtly present in small groupings within the radar-bright regional plains materials, although they are not as apparent as on regional plains elsewhere on Venus. Most structural features within the quadrangle appear to be concentrated within the linear belt regions and surrounding coronae and coronalike features.

Isolated patches of material are correlated with the various regional plains units on the basis of similar radar properties even though the correlation cannot be proven due to lack of outcrop continuity.

The local plains materials differ from regional plains materials primarily in their limited area and very localized distribution. Local plains materials include textured plains material (unit pt), mottled plains material (unit pm), and smooth plains material (unit ps).

Textured plains material (unit pt) is present both within and outside of linear belts. Within linear belts it occurs as small, elongate patches. It is devoid of any resolvable structural patterns. The material has a textured appearance which is either the result of a small-scale dense structural fabric below the radar resolution or homogeneous roughness. The textured plains material is interpreted to be younger than both the regional plains and linear belt materials.

Mottled plains material (unit pm) also is found both within and outside of the linear belts. It is characterized by a small-scale (20 km) blotchy pattern of moderately bright to moderately dark patches inferred to be due to abundant small shield volcanoes and associated flows. The scalloped edges of the unit boundaries are interpreted as juxtaposed shield flows. Owing to the consistent roundness of the scallops and the absence of cross-cutting structures, the mottled plains material is interpreted to be younger than both adjacent regional plains and linear belt materials.

The smoothest and least widespread of all material units within the quadrangle is smooth plains material (unit ps). Small patches of smooth plains material are concentrated in the southern part of the quadrangle near southern Pandrosos Dorsa and Neyterkob Corona. It is characterized by both its radar-dark backscatter (–11.499 dB) and its jagged edges, which embay all of the surrounding materials. Smooth plains materials are superposed on digitate flows, dark regional plains, and all linear belt materials.

FLOW MATERIALS

Within the Pandrosos Dorsa quadrangle are four types of flow materials defined by their morphology on the SAR images: four lobate flows (unit flb); a lineated flow (unit flt); seven digitate flows (unit fd); and two flowlike deposits (unit fs) inferred to be due to slump associated with a volcanic feature. Each of the mapped flow units has a separate source, and thus it is unclear if the compositions of the materials are similar. Where distinctly separate units of flows share a contact, an age relation cannot be determined. The map shows dashed contacts within units where this occurs.

Lobate flow material (unit flb) is characterized by overall homogeneity with regard to texture and radar brightness. The unit contains faint traces of lobate forms throughout and has moderate radar backscatter. In some places, generally at the leading edges of the material unit, the lobate forms are more easily recognized due to their highly variable backscatter coefficients (–6.971 dB to –12.281 dB), which generally contrast greatly with the surrounding materials. Most of the mapped lobate flows originate from regions outside the quadrangle boundaries. Flow directions are evident from lobate forms within the unit and are consistent with present topographic slopes. Locally, the lobate flow material appears to be superposed on the regional plains material, but this distinction is too unclear to be definitive.

Also present in the quadrangle is a single deposit of lineated flow material (unit flt) located at 73.0° N., 238.7° E. The backscatter coefficient is very bright (–5.525 dB) but the origin of this brightness is different in the northern and southern parts of the mapped unit. The southern half of the lineated flow has a fan-shaped morphology and a knobby or hummocky texture that is responsible for its radar brightness. In the northern half, the material is concentric to its source, and the radar brightness is created by sets of orthogonal radar-bright linear features. Due to morphologic differences, the two flow forms are interpreted to have been deposited at different times. The apparent source is outlined by the shape and direction of the flows, but the actual source is no longer visible. The lineated flow material is superposed on lobate flow material.

Digitate flow material (unit fd) is characterized by elongate individual flows that intermingle with fingerlike morphology. The backscatter coefficients vary greatly from very bright (–7.888 dB) to moderately dark (–10.129 dB), indicating highly variable surface roughness. Of the seven digitate flows, four appear to originate in regions that are dotted with volcanic shields and where the material flow direction is clearly outward from the approximate center of the shield fields. The remaining three mapped flows originate either from a single volcanic source or from a source that is no longer visible. Each of the digitate flows is younger than regional plains. Where one of the digitate flows (Turgmam Fluctus) comes in contact with Lonsdale crater, the crater outflow embays the digitate flow, thus indicating that the crater outflow material is younger. The digitate flow material is superposed on the lobate flow material, as is indicated east of Nyterkob Corona where the digitate flow material is controlled by wrinkle ridges in the lobate flow material.

Slump material (unit fs) occurs as two small patches near 71°–72° N., 198° E. It is characterized by a curvilinear pattern of radar bright linear features and appears to be associated with digitate flows that surround it. Its radar brightness (–7.244 dB) is inferred to result from the radar bright linear features that are in turn inferred to result from slump activity along the edge of the small volcanic center east of the patches. The slump material unit is younger than the regional plains, but its upper stratigraphic limit is indeterminable.

CORONA MATERIALS

Portions or all of nine coronae are present within the quadrangle. Concentric annuli and radial structures that define the coronae are discussed in the section "Structural Geology". Three separate material units are related to these coronae, the relative ages of which are unknown. Not all coronae have associated corona materials; some of the coronae within the Pandrosos Dorsa quadrangle are structural features alone, with no evidence of associated deposits (for example, Aspasia Corona). Corona materials are superposed on all regional plains materials.

Corona material c (unit co_c) lies within and near annuli of Neyterkob, Cassatt, and Muzamuza coronae, and an unnamed corona centered at 69.9° N., 198.9° E. This material is differentiated from corona material b in that corona material c has a brighter backscatter coefficient (–6.757 dB) and a prominent structural pattern that resembles tessera material. It is differentiated from tessera material by its distinct association with coronae features.

Corona material b (unit co_b) is characterized by a moderately dark backscatter coefficient (–11.803 dB) and digitate and lobate patterns that appear to originate at corona features. The corona flow materials of Cassatt, Muzamuza, Ninkarraka, and Schumann-Heink appear to mostly surround the coronae, which indicates little topographic variation across the affected region at the time of emplacement. Other corona material b flows do not entirely surround the associated corona structures.

Corona material a (unit co_a) is characterized by a homogeneous textured appearance and a moderately bright backscatter coefficient (–9.467 dB). The unit is within coronae annuli and tends to follow the concentric pattern of the coronae structures. This material is associated with Neyterkob, Cerridwen, Cassatt, and Muzamuza coronae, and an unnamed corona centered at 69.9° N., 198.9° E.

IMPACT CRATER MATERIALS

Deposits of twelve impact craters are present within the quadrangle. These include Barsova, Dolores, Evangeline, Lonsdale, Orlova, Zoya, Ahava, Batya, Elizabeth, Ezraela, Kelila, and Yetta. Impact crater deposits include undifferentiated material of central peaks, floors, rims, and ejecta blankets (unit c), and fluid flow material (unit cf). Most of the materials included within the undifferentiated crater material have high radar cross sections due to the surface roughness. As with digitate flows, some of the flow materials have lower radar cross sections.

All of the craters are younger than the regional plains. Flow material extending westward from Lonsdale appears to embay eastwardly flowing digitate material of Turgmam Fluctus which originates at a shield field within Iris Dorsa. This relation indicates that Lonsdale is demonstrably younger than Turgmam Fluctus. Lack of direct contact between other craters and digitate flows prohibits further stratigraphic correlation. The flows from the crater Barsova follow the broad rise of Iris Dorsa and flow in a southeasterly direction as indicated by the digitate pattern. This relation implies that Iris Dorsa was elevated prior to the impact that formed Barsova.

Also of interest is the asymmetric crater Dolores, at 51.5° N., 201.6° E. The southern part of its rim is missing or obscured. If the rim is missing because it is covered by the surrounding regional plains materials, then the crater would be older than these plains. However, a zone of ejecta avoidance south of the rim of Dolores suggests a low angle impact from the south (Schultz, 1992), which also could result in an incomplete rim. The low angle impact is further supported by the butterfly ejecta pattern (Gault and Wedekind, 1978). Wrinkle ridges superposed on regional plains southeast of the crater rim appear to constrain flow material from Dolores, indicating that the wrinkle ridges, and thus the regional plains, must be older than the crater. Therefore, the regional plains material cannot be superposed on the southern part of the crater rim, and thus the crater clearly is younger than regional plains.

The lack of contacts with any material other than regional plains leaves the upper stratigraphic age limits of the remaining impact craters unconstrained. Also present are two "splotch" features centered at 51.5° N., 215.2° E. and 54.3° N., 196.0° E. Splotches are believed to be the result of near-surface explosions of bolides that deposited fragmented material without actually reaching the surface (Campbell and others, 1992). These splotches also are younger than the regional plains.

SURFICIAL MATERIALS

Several local regions within the quadrangle appear to have undergone at least some aeolian activity, represented on the SAR images by 1) feathery, diffuse swaths bordering individual ridges toward the southernmost part of the quadrangle, or 2) diffuse patches overprinting regional plains materials near 53° N., 183° E., 69° N., 180° E., and 73° N., 195° E. Both types probably represent very thin veneers of reworked older materials.

STRUCTURAL GEOLOGY

The Pandrosos Dorsa quadrangle contains numerous structural features: large linear belts, small structures confined to the large belts, wrinkle ridges, radar-bright linear features, and coronae and coronalike features. The dominant structural features are the twelve linear belts and their contained ridges and radar-bright linear features. This section includes a general overview of these belts, including a detailed analysis of the southern part of the most complex belt, Pandrosos Dorsa. This discussion is followed by descriptions of the other structural features.

LINEAR BELTS

Linear belts are defined as large-scale linear zones that contain and confine smaller scale structures. Owing to the combined effects of topography and roughness on radar backscatter, linear belts tend to be much brighter on SAR images than the surrounding plains materials. Structures related to linear belts have two different scales: long wavelength, representing the spacing between belts; and short wavelength, representing the spacing between the smaller structures confined to the individual belts. Belts are generally categorized by the type of short wavelength structures that they contain (for example, ridges or radar-bright linear features). Linear belts commonly are elevated relative to surrounding plains (Solomon and others, 1992; Squyres and others, 1992); however, due to topographic variations along the lengths of each belt, elevated topography is not a defining characteristic within the Pandrosos Dorsa quadrangle.

Linear belts occur in low-lying plains, specifically within Lavinia, Atalanta, and Vinmara Planitiae (Solomon and others, 1992). Initial studies of linear belts were based on Venera 15 and 16 images (Barsukov and others, 1986; Basilevsky and others, 1986; Kryuchkov, 1988; Sukhanov and Pronin, 1989; Sukhanov and others, 1989; Frank and Head, 1990) and Arecibo images (Campbell and others, 1991; Senske and others, 1991). The low resolution of these datasets made distinction between different styles of short-wavelength structures within the belts difficult, if not impossible. In most cases, the higher resolution Magellan data allow for clearer distinction between radar-bright linear features and ridges.

The apparently very low rate of deposition and erosion on Venus leads to the inference that most ridges and other narrow linear features are primary structures. These structures are inferred from their morphologies, as seen on the SAR images. Ridges are identified on cycle 1 SAR images by brightness along the west edge and darkness along the east edge, separated by a transitional region of intermediate radar brightness. This gradual transition from radar bright to radar dark across the crest indicates that the ridges have gentle curvatures. If these ridges are primary fold structures, as is generally inferred, then the folds are gentle and open, consistent with a simple buckling genesis. Radar-bright linear features are generally interpreted as fractures or faults, an inference supported by places where they are wide enough to resolve bright and dark scarps defining a grabenlike depression. On the basis of Venera 15 and 16 images, the belts in the Vinmara Planitia region were referred to as the Ridge Belt Plains-Fan Assemblage (Frank and Head, 1990). All but one belt were classified by Frank and Head (1990) into Class II, defined as belts that generally consist of a multitude of closely spaced smaller ridges (Kryuchkov, 1988). The one exception is Lukelong Dorsa, which was classified as a Class I belt, defined as swells with broad summits (Kryuchkov, 1988).

In comparison to the clearly defined belts of Lavinia Planitia, the belts of Vinmara Planitia are not exclusively ridge or fracture belts. Nor do the belts of Vinmara Planitia display the orthogonal pattern observed in Lavinia Planitia, where ridge and fracture belts are about normal to each other (Squyres and others, 1992). Rather, in Vinmara Planitia, most of the linear belts are composite or hybrid belts consisting of ridges, fractures, and grabens. Hence the more general and nongenetic term "linear" belts is preferred to "ridge" or "fracture" belts.

Although analysis of Magellan images indicates that many of the short-wavelength structures confined to the linear belts are not ridges, the previously described closeness and regularity of spacing between structures holds true. As noted by Zuber and Parmentier (1990), the distance between linear belts also tends to be uniform. The structures within the belts deform a variety of material units, including older material of unknown origin, younger regional plains materials, and patches of tessera.

Long-Wavelength Deformation

In plan view, the twelve linear belts of the Pandrosos Dorsa quadrangle bifurcate and merge along strike, thereby forming an anastomosing pattern having an overall north-south orientation. Belt lengths range from 1,000 to 2,500 km; widths range from 20 to 230 km. Characteristic spacing between the belts is 300–400 kilometers, increasing southward because of the general north-south orientation of the belts, which creates the fanlike pattern noted by earlier workers. Each of the belts is surrounded by regional plains material, and one of the belts comes in direct contact with a major block of tessera material present in the quadrangle.

Although the spatial resolution of altimetry data from Magellan is superior to that of prior missions, the altimetry footprints in the quadrangle range from 209 km² in the south to 345 km² in the north, areas that are large relative to the widths of short-wavelength structural features. Thus the resolvable topographic expressions of linear belts reflect only the belt-scale morphologies of these features. Ten of the twelve belts have elevated topography relative to both the surrounding plains materials and the mean planetary radius, although some parts of these belts show no relief at all (fig. 2). Whereas Lukelong and Laūma Dorsa are each associated with linear troughs, only Laūma Dorsa is topographically depressed in its entirety relative to the surrounding plains. A variety of linear belt styles is revealed from topographic profiles along transects drawn perpendicular to the trend of each belt (figs. 3, 4). Of the twelve linear belts of the Pandrosos Dorsa quadrangle, Lukelong, Laūma, Anpao, Pandrosos, Iris, and unnamed Dorsa are most illustrative of the variety of styles present among linear belts and provide the most important information for determining geologic history in the region.

The southern third of Lukelong Dorsa is in the northwest corner of the Pandrosos Dorsa quadrangle. The total length of Lukelong Dorsa is 1,560 km, and it has a relatively constant width of 50 kilometers. The belt trends approximately northwest. Unlike most linear belts on Venus, which are generally elevated relative to surrounding plains, Lukelong is contained within a trough approximately 100 km wide and 600 m deep relative to the average elevation of the surrounding plains (fig. 4*A*). The belt also is structurally simpler than most of the other belts within the Pandrosos Dorsa quadrangle, because the trends of the included ridges and linear features are generally parallel to the trend of the belt and lack the complex anastomosing patterns seen in the other belts.

In the western part of the quadrangle, Laūma Dorsa merges with Lukelong Dorsa at 65.5° N., 186° E. Laūma Dorsa is 2,480 km long and ranges in width from 32 to 89 km. Laūma Dorsa is oriented north-south throughout its entire length, and it is the longest and straightest belt within the quadrangle. Together, Lukelong and Laūma define the boundary between Atalanta Planitia to the west and Vinmara Planitia to the east.

In addition to the abundance of radar-bright linear features and short-wavelength ridges, Laūma contains Aspasia Corona and an abundance of ovoid structures elongated parallel to the trend of the belt. Although these ovoid structures are concentrated in the south, they are present along the entire length of the belt. Fractures and grabens are not observed anywhere within Laūma Dorsa.

Similar to Lukelong Dorsa, Laūma Dorsa occurs within a linear trough reaching depths of approximately 600 m below the surrounding plains material and over 1 km below the mean planetary radius (fig. 4*B*). The trough is asymmetric, reaching greatest depths along the eastern edge of the belt.

Anpao Dorsa, near the longitudinal center of the quadrangle at 205° E., forms the northern extension of the wide southern part of Pandrosos Dorsa. The belt is oriented north-south, is 920 km long, and has a maximum width of 78 km. It contains radar-bright linear features, fractures, ridges, and grabens, which categorize the belt as a hybrid linear belt. Topographically, Anpao Dorsa is asymmetric with a deep trough on its west edge and broad ridge along its crest (fig. 4*C*).

Pandrosos Dorsa is near 205° E. and is primarily oriented north-south, but its orientation changes to N. 10° E. at 58.3° N., 207° E. where the belt splits to form Anpao Dorsa to the west and the continuation of Pandrosos Dorsa to the east. The length of the belt is approximately 2,190 km, and its width changes from 62 km in the north to 229 km in the south. The belt contains linear features, fractures, ridges, and grabens, thus categorizing it as a hybrid linear belt. Details of the internal structures of Pandrosos Dorsa are addressed as a separate analysis in the "Discussion" section.

Contained within the southern part of Pandrosos Dorsa is a shield field from which the digitate flows to the east of the belt emanate. Topographically, Pandrosos is asymmetric and quite complex, having an undulating pattern of ridges and troughs across its crest (fig. 4*D*, 4*E*). Figure 4*E* shows a profile across the widest part of southern Pandrosos Dorsa. From west to east the transect reveals a low, broad ridge, approximately 100 km across, followed by two ridges; one narrow and low, the other broad and high. At its apex, Pandrosos reaches 6053.3 km, the highest elevation of any belt in the quadrangle.

Iris Dorsa, near 58° N., 217° E., extends as far north as 65.5° N. and as far south as 48° N., just beyond the quadrangle boundary. Iris is 1,790 km in long and ranges from 57 to 92 km wide. Its strong anastomosing pattern creates a belt orientation that varies from the dominant north-south to N. 10° E. and N. 10° W. Whereas the northern part of the belt is dominated by short-wavelength ridges, the southern part resembles a hybrid belt, containing both ridges and radar-bright linear features. As with Pandrosos Dorsa, digitate flows emanate from the center of Iris Dorsa. Topographically, Iris has the smoothest profile of any of the belts in the quadrangle, as it forms a single broad ridge as opposed to a series of parallel ridges. A trough along the west edge of Iris is present only in the northern parts of the belt.

An unnamed hybrid linear belt is present in the northeastern part of the quadrangle, centered at 68° N., 231° E. It is oriented N. 10° W., is approximately 1,600 km long, and has a relatively constant width of 85 km. Whereas the northern part of the belt is surrounded by regional plains materials, the southern part of the belt terminates within Virilis Tessera. Evidence that formation of the belt postdates formation of Virilis Tessera material is observed where tessera material contained within the belt is cut by belt structures and elongated parallel to the trend of the belt. The topographic expression of this linear belt resembles that of Pandrosos Dorsa in that it consists of multiple ridges and troughs, and the highest elevation is reached at the east edge.

Short-Wavelength Deformation

Each of the long-wavelength linear belts contains numerous short-wavelength deformation features. Two types of structures are observed: ridges, interpreted as folds resulting from contractional strain; and radar-bright linear features, interpreted as fractures and faults resulting from extensional strain (Solomon and others, 1991). The short-wavelength structures that are resolvable as ridges reach lengths of 200 km and widths of 30 km and average approximately 150 km and 15 km, respectively. The linear features range in length from tens to hundreds of kilometers. The ridges and linear features have a regular spacing of 25 km. Locally, the linear features are wide enough to be recognized as grabens. In plan view, the individual ridges are somewhat sinuous, whereas the fractures are straight to gently curved.

Linear belts are structurally complex. Some linear belts change along their lengths from being dominated by ridges to being dominated by fractures and grabens. Other belts are hybrids or composites of ridges, fractures, and grabens. In many places within the hybrid belts, ridges and fractures are oriented subparallel to each other and to the long axis of the belt. The clearest example of this relation is seen in the southernmost part of Pandrosos Dorsa, where individual ridges and fractures are oriented within 10° of north-south and within 5° of each other.

Elsewhere, ridges and fractures are not parallel to each other. For example, fractures present in the central part of Iris Dorsa (58° N., 217° E.) are oriented 55° east of the north northeast to south-southwest trending ridges. Farther north, where Iris Dorsa merges with Akuanda Dorsa, pervasive fractures are oriented approximately 90° from the ridges. Here the fractures can be followed across the broad arches of the north-northwest to south-southeast trending ridges indicating that either the fractures are superposed on the preexisting ridges or that the fractures formed before the ridges and are undisturbed due to the extremely gentle folding process.

In addition to the grabens recognized within the linear belts, a second set of grabens is observed bounding the edges of Pandrosos Dorsa and extending into the regional plains materials. These grabens are as long as 600 km and tend to take many sharp turns along their lengths. Their presence in the regional plains material indicates that they are younger than grabens restricted to the deformation belt materials.

Also of significance are relations between the short-wavelength ridges and the tessera material. As discussed in the previous section, the unnamed dorsa in the northeast corner of the quadrangle appears to deform large blocks of tessera material that now occur as elongate strips with orientations parallel to that of the belt. In other places, tessera material contains short-wavelength ridges that parallel those of a nearby linear belt. An example of this relation occurs near 56° N., 198° E., where a block of tessera material contains broad north-south trending ridges spaced 30 to 40 km apart.

WRINKLE RIDGES

Wrinkle ridges are sinuous, radar-bright linear features that range in length from the lower limit of resolution (about 1 km) to hundreds of kilometers, and generally are less than 1 km wide. They are abundant on most of the plains of Venus (Solomon and others, 1992; Squyres and others, 1992; Bilotti and others, 1993) and are widespread, visible, and bright in the neighboring quadrangles within the same latitude range (Atalanta Planitia to the west and Metis Regio to the east). But wrinkle ridges are rare within the Pandrosos Dorsa quadrangle and only locally approach the density and brightness of wrinkle ridges on regional plains elsewhere. Where wrinkle ridges are present, they appear faint on the SAR images and follow only a single orientation within a defined region. However, on a quadrangle scale there is no consistent orientation of wrinkle ridges.

Some of the wrinkle ridges are adjacent to or included within linear belts. For example, wrinkle ridges west of Ahsonnutli Dorsa (73.0° N., 201.5° E.) parallel short-wavelength ridges within the belt. Along Laūma Dorsa, wrinkle ridges appear to mimic the trends of the radar bright linear features and ridges that comprise the belt. The similarity in spacing and orientation of wrinkle ridges and short-wavelength structures within the deformation belts implies similar stress orientations and suggests the possibility that linear-belt ridges could have evolved from wrinkle ridges.

In other parts of the quadrangle, however, wrinkle ridges and short-wavelength structures are not parallel. For example, in the region near 50°–53° N., 195°–205° E., wrinkle ridges within regional plains materials intersect ridges within the nearby linear belts at an angle of approximately 30°. The absence of cross-cutting relations between the wrinkle ridges and the ridges in this region prohibits determination of a sequence of events.

RADAR-BRIGHT LINEAR FEATURES

Radar-bright linear features too narrow (<1 km wide) to be resolved clearly by Magellan radar are abundant in the Pandrosos Dorsa quadrangle, as they are elsewhere on Venus. These narrow features occur within linear belts, across sections of regional plains, and surrounding coronae and coronalike features. Locally, small sections of the longer radar bright linear features are wide enough to be recognized as grabens, thus implying that the linear features are extensional along their entire lengths and that parallel members of the same set of linear features also are extensional. Where geometric evidence for extension is not visible, however, some of these radar-bright linear features may be very narrow ridges.

The radar-bright linear features within the quadrangle range in length from tens to hundreds of kilometers and define various patterns. Between the linear belts, sets of long, parallel, widely spaced linear features cut across large sections of the regional plains. Examples can be seen as east-west-trending features near 61.0° N., 217.0° E. and 57.5° N., 226.0° E. Other linear features occur as radial and concentric sets around coronae and coronalike features. Aspasia Corona provides a good example of a concentric set, whereas Cassatt Corona provides a good example of both radial and concentric sets. A radiating lineament system centered at 63.7° N., 195.0° E. is interpreted as the surface manifestation of shallow, laterally emplaced dikes that radiate from a magma reservoir beneath the central circular fracture pattern (Grosfils and Head, 1994). The curved lineaments radiating from the central structure extend to distances of 450 km from the central shallow depression. The radiating lineaments cross-cut surrounding regional plains and the large block of tessera to its east, implying the lineaments post-date these material units. With respect to the structures of Laūma Dorsa, however, the radiating lineaments are both throughgoing and deflected, implying that deformation of Laūma Dorsa started before formation of the lineament system and continued after its cessation (Grosfils and Head, 1994).

CORONAE AND CORONALIKE FEATURES

The nine coronae within the quadrangle exhibit various topographic and structural features that meet the corona classification of Stofan and others (1992). Those referred to in this section as "coronalike" features also meet the characteristic qualifications of coronae (Stofan and others, 1992; Squyres and others, 1992) but are presently uncataloged. The interiors of those coronae that are fully present within the quadrangle boundaries are relatively simple compared to larger coronae on the planet's surface. There is no spatial pattern identified in the distribution of the coronae within the Pandrosos Dorsa quadrangle as is apparently displayed along Parga Chasma in the southern hemisphere (Chapman, 1999) and elsewhere on Venus (Stofan and others, 1992; Squyres and others, 1993).

Corona diameters range from about 45 km to more than 200 km. Five coronae (Cassatt, Muzamuza, Ninkarraka, Nyterkob, and Cerridwen) fall into the concentric class of Stofan and others (1992), two (Nzingha and Aspasia) are asymmetric coronae, and Shumann-Heink is a domical corona. Four of the coronae occur as linked pairs: Cassatt and Muzamuza in the north-central part of the quadrangle, Cerridwen and Nyterkob straddling the south boundary of the quadrangle. Aspasia is astride the southern part of Laūma Dorsa, and the Cassatt/Muzamuza pair occurs at the north end of Anpao Dorsa. The other coronae do not appear to be spatially related to major structural features.

VOLCANIC FEATURES

Present within the Pandrosos Dorsa quadrangle are three distinct classes of volcanic features: flow materials, small shields, and lava channels. The flows are present as digitate, lobate, lineated, and slumped materials, and are described in detail in the stratigraphy section. The small shield volcanoes occur in three styles in the Pandrosos Dorsa quadrangle: as coalesced shields forming mottled plains (for example, unit pm), as clusters of shields forming volcanic shield fields, and as isolated shields. The following is a description of the variety of small shields and the single lava channel present in the quadrangle.

The first style of shield volcanoes, mottled plains, is considered a stratigraphic material unit because the flows emanating from the individual shields are extensive enough to completely cover the region in which they are situated. The description of this style is therefore found in the local plains materials section of the stratigraphy section.

The second style, volcanic shield fields, differs from the regions of mottled plains in that the flows of shield fields do not have contrasting radar coefficients and are not voluminous enough to merge with one another. Shield fields are defined by distinct clusters of volcanic domes and shields with diameters of 5-10 km. Some of these have central pits. In the Pandrosos Dorsa quadrangle, many of the shield fields are within linear belts, an occurrence that has prompted arguments for an extensional origin for these belts (Sukhanov and Pronin, 1989). Because the flows from shield fields do not completely cover the region in which they are situated, they are not considered a stratigraphic material unit and are delineated on the map by a stipple pattern.

The third style of volcanic shields includes a number of small, individual shield volcanoes not readily associated with other shield volcanoes or regions of intense deformation. These small shields appear to have low relief and some surrounding flank materials, but they are too small to be resolved on topographic maps and thus to distinguish them as volcanic edifices (Aubele, 1993).

The isolated shields are readily visible on the SAR images, because the radar backscatter properties of their flows contrast with those of the surrounding plains materials and because of the contrast in radar brightness of their west and east flanks. Genetically, they are not necessarily different from those small shield volcanoes that cluster to form mottled plains.

Part of a lava channel is present in the southwest corner of the quadrangle (50°–52° N., 180°–183° E.). This channel, the longest present on the surface of Venus, is nearly 6,800 km long and has a nearly constant width of 1 to 3 km (Baker and others, 1992). It is classified as a canali-type simple channel and is inferred to have formed from lava that originated at a volcanic construct at 44.5° N., 185° E. (Baker and others, 1992). Owing to its enormous length, this lava channel provides relative age relations for many material units through which it passes. The section of the channel present in the study area incises radar-dark regional plains but is filled by radar-bright regional plains. This relation indicates that the channel formed while regional plains were being emplaced; after emplacement of radar-dark regional plains but before emplacement of radar-bright regional plains.

DISCUSSION

Puzzling issues related to the deformation within the Pandrosos Dorsa quadrangle include the origin of the linear belts, especially the dual-wavelength spacing, and the origin of the subparallel ridges and linear features within the belts. Geologic and structural mapping of the Pandrosos Dorsa quadrangle has revealed evidence that both supports and conflicts with some of the previously suggested origins for the latter. An important conclusion of this study is that tectonism is progressive on Venus, at least within Vinmara Planitia.

The characteristic dual wavelength spacing between linear belts and between individual ridges within these belts (referred to in this study as "long-" and "short-wavelength" deformation) implies buckling of flexurally strong upper crust and upper mantle separated by a zone of weakness in the lower crust (Banerdt and Golombek, 1988; Zuber, 1987; Zuber and Parmentier, 1990). These models imply belt-normal contraction, and most models for the origin of the long-wavelength linear belts on Venus involve belt-normal lithospheric shortening and crustal thickening (Basilevsky and others, 1986; Zuber, 1987; Frank and Head, 1990; Phillips and others, 1991).

One of the more apparent and perplexing problems with the generally accepted contractional origin of the linear belts is the presence in most of the Vinmara Planitia belts of subparallel structures that are interpreted to result from both extension and contraction. Previous studies inferred that the "ridge" and "fracture" belts of Lavinia Planitia resulted from belt-normal shortening and crustal thickening based on the large-scale geometric similarities of the two types of linear belts and the observation that some belts transform from ridge to fracture morphology along their lengths (Squyres and others, 1992), albeit with approximately orthogonal orientations. The linear belts of Vinmara Planitia differ from those of Lavinia in that they are hybrid belts that contain interspersed structures interpreted to result from both extensional and contractional strains. The two types of structures are commonly oriented subparallel to each other and to the long axes of the belts themselves. The complex history of southern Pandrosos Dorsa, discussed in the following paragraphs, provides important data on the sequence of deformational events and thus provides a useful constraint on genetic models for linear belts.

Pandrosos Dorsa contains four stratigraphic units; linear belt materials a and b, tessera material, and smooth plains material (fig. 5). Linear belt materials a and b are characterized by north-south-trending ridges having similar morphologies and similar spacing of 5–7 km, thus suggesting that ridge formation in both materials was the result of a single deformational event (fig. 6). However, only belt material b contains pervasive fractures, which are oriented from north-northeast-south-southwest to north-south, generally parallel to the ridges (fig. 6). Where radar-bright linear features are not exactly parallel to the ridges in belt material b, two crosscutting relations exist. In some localities the radar-bright linear features cut across the smaller ridges. This relation can form by preexisting fractures being folded during later contraction or from the fractures occurring after the folds. The resolution of the images is not sufficient to distinguish these two cases, and thus a sequence of events cannot be determined. Elsewhere, the radar-bright linear features appear to abut the flanks of the ridges. Whereas this relation may initially suggest that the folds formed prior to the fractures, it can be explained by younger flooding of only some of the topographic lows between ridges. This selective flooding will result in fractures apparently terminating against ridges because the fractures are present on unflooded sides of ridges but buried on flooded sides. The fractures and ridges were originally mutually intersecting and thus of ambiguous relative age. Consequently, crosscutting relations and truncation of structures are not useful tools for determining the sequence of deformational events in Pandrosos Dorsa.

The stratigraphic relations among the geologic units of Pandrosos Dorsa imply that the pervasive fractures formed before formation of the north-south ridges. The older belt material b was deposited and fractured before the deposition of belt material a. Following fracture formation but before ridge formation, the western half of the belt was flooded by belt material a, burying both material b and the fractures. Following deposition of belt material a, contractional ridges were formed in both units within the belt. This sequence is supported by topographic data (figs. 3, 4*E*) which show that exposed belt material b is elevated approximately 0.8 km above belt material a, a morphology that allows the pervasive fractures to remain present within high-standing belt material b while being obliterated by the deposition of the material forming belt material a within the lower part of the belt.

Most models for the origin of linear belts assume belt-normal contraction accompanied by crustal thickening, consistent with the dual wavelength spacing of structures. The stress responsible has been explained as due to convective downwelling centered beneath low-lying plains regions (Zuber, 1990; Bindschadler and others, 1990; Phillips and others, 1991). A contractional origin was initially supported by the apparent morphological similarity of linear belts to lunar, mercurian, and martian wrinkle ridges (Barsukov and others, 1986; Frank and Head, 1990), which commonly consist of broad arches with a superposed single, narrow sinuous ridge. However, Magellan images indicate the ridges of linear belts are morphologically dissimilar to wrinkle ridges (Banerdt and others, 1997). Support for crustal thickening is found in the tendency for the belts to be elevated with respect to the surrounding plains materials (Solomon and others, 1992; Squyres and others, 1992), although not all belts or all parts of belts are elevated in the Pandrosos Dorsa quadrangle. An alternative extensional origin has been proposed by Sukhanov and Pronin (1989), who noted that some belts contain volcanic centers that are difficult to justify in a contractional environment. Sukhanov and Pronin (1989) interpret Lukelong Dorsa as a linear diapir and Laūma Dorsa as a region where structures are streamlined around preexisting domes. Supporting evidence, such as volcanic flooding in troughs of Lukelong Dorsa and volcanic domes along the entire length of Laūma Dorsa, is lacking. In addition, their model does not account for the broad archlike ridges that are characteristic of most belts and suggestive of contractional strains.

Three models have been suggested for the presence of extensional fractures within linear belts: extension due to local igneous intrusion and lithospheric heating (Solomon and others, 1992); stretching of a brittle surface layer over a contractional structure (Squyres and others, 1992); and gravitational collapse of the upper crust (Phillips and Hansen, 1994). Of these models, the first two were suggested for the origin of "fracture belts" of Lavinia Planitia in which only fractures are present within the belts. These models are not discussed further because they do not incorporate or explain the presence of ridges and thus do not explain the apparent shortening in the belts of Vinmara Planitia. Only the Phillips and Hansen model is applicable to the coexistence of subparallel ridges and fractures. In this model, the crust collapses when relief due to crustal thickening produces gravitational stresses sufficient for failure.

The geologic relations within the Pandrosos Dorsa quadrangle reveal some shortcomings of the gravitational relaxation model. The model predicts that the contractional ridges should predate the extensional linear features, whereas stratigraphic evidence, especially within Pandrosos Dorsa, indicates that the opposite is true. The extensional structures of Pandrosos Dorsa may be relics of a regionwide event predating the formation of the linear belt, but no evidence exists for extensive early fracturing of comparable relative age external to the belt. Laūma Dorsa also presents a problem for the gravitational collapse model because most of it is lower than surrounding plains, not higher. Therefore, if gravitational relaxation is the true mechanism of formation for Laūma Dorsa, a formerly elevated belt dominated by ridges must have undergone collapse that brought its elevation lower than the horizontal level at which the materials originated, a result more consistent with extension and crustal thinning than with the contraction and crustal thickening required to account for the ridges.

The geology of the linear belts indicates that Vinmara Planitia underwent extensive and prolonged tectonism. Embayment relations between most of the materials within the linear belts and the surrounding regional plains materials suggest that most belts began forming before emplacement of regional plains materials. However, Laūma Dorsa deforms the relatively young radar-bright regional plains material and therefore formed during or after emplacement of this plains material. Lancaster and others (1995) interpreted the radar-bright plains material near Laūma Dorsa as a post-regional plains sheet flow emanating from Laūma Dorsa and some nearby east-west-trending fissures. This alternate interpretation does not change the inference that linear belt deformation within the Pandrosos Dorsa quadrangle has been progressive, because both interpretations imply deformation within Laūma Dorsa after emplacement of most or all regional plains materials.

Additional evidence in support of prolonged long-wavelength deformation is the stratigraphic and morphologic relation between radar-bright and radar-dark regional plains materials. In the plains region between Pandrosos Dorsa and Bathkol Tessera the younger radar-bright regional plains material occurs in the longitudinal center of radar-dark regional plains material (approximately centered at 204° E.), implying that a linear depression formed after the dark plains material was deposited and before the bright regional plains material was emplaced (fig. 7). Thus, the stresses forming the long-wavelength deformation also were progressive with respect to emplacement of regional plains materials.

GEOLOGIC HISTORY

The geologic history of the Pandrosos Dorsa quadrangle begins with the formation and deformation of tessera material. Embayment and truncation relations indicate that tessera material is the oldest material within the quadrangle. However, tessera materials may not be the oldest materials planet-wide, and all tessera patches and blocks need not be stratigraphically correlated. The characteristics of tessera material before it was deformed are unknown.

Densely lineated material, present as radar-bright inliers, also is interpreted as relatively old. In places, densely lineated material occurs at the edges of the tessera blocks, embaying the tessera material and truncating structures within the tessera. The common azimuth of fractures in most patches of densely lineated material suggests regional continuity of deformation. These fractures are truncated by and thus older than surrounding regional plains materials. It is not possible to infer the elapsed time between the emplacement and deformation of tessera material and the emplacement of densely lineated material, or between either of these units and the emplacement of surrounding plains materials.

Most of the linear belts contain materials that are older than the surrounding regional plains materials, as indicated by the superposition of plains materials on belt materials and on the ridges and linear features deforming the belt materials. The origin of belt materials is inferred to result from an earlier episode of plains emplacement, although no direct evidence exists for correlative materials beneath presently exposed regional plains materials. Ridges within one linear belt, Laūma Dorsa, also deform the youngest regional plains material.

The emplacement of regional plains was approximately coeval with the deformational event that formed the linear belts. This scenario may imply rapid emplacement of regional plains or prolonged deformation, or both, but owing to the extensiveness of the regional plains materials beyond the boundaries of the study area and to indications of continued large-scale deformation after regional plains deposition (Laūma Dorsa), prolonged deformation is preferred. Radar-bright regional plains materials locally fill grabens and part of the lava channel cutting radar-dark regional plains, relations that suggest at least two episodes of widespread plains emplacement. Although the sparsity of pervasive wrinkle ridges on the regional plains tends to distinguish these plains from most regional plains elsewhere on Venus, these plains are otherwise similar to and areally continuous with regional plains in adjacent quadrangles. Thus they most likely formed during the near-global resurfacing event of approximately 200–600 million years ago (Strom and others, 1994). Formation of coronae and coronalike features was either coeval with or immediately followed regional plains emplacement, or both.

Although geophysical models (Banerdt and Golombek, 1988; Zuber, 1987; Zuber and Parmentier, 1990) imply a similar age, the temporal relation between the two wavelengths of deformation characteristic of the linear belts cannot be resolved geologically. Resolution of this ambiguity will be important for understanding the causes of the structures confined within the belts.

Deformation of a lesser intensity continued after formation of the regional plains, further indicating progressive deformation in the region. The absence of radar-bright linear features or folds within digitate flows, lobate flows, and smooth local plains material indicates that these materials were emplaced after formation of the structures affecting regional plains. Although each of these flows is younger than the surrounding materials, they are not necessarily coeval; multiple episodes of volcanism are more likely. The embayment relation between Turgmam Fluctus and Lonsdale crater indicates that this digitate flow is older than the formation of Lonsdale. However, the stratigraphic relation from this single occurrence cannot be applied to the other digitate flows and craters in the quadrangle because they are not in direct contact with one another.

Impact of all craters and their associated flows followed regional plains emplacement. Flows from Dolores crater were diverted by and are thus older than nearby wrinkle ridges; the ages of other craters relative to these structures are not known.

The geologic history of the Pandrosos Dorsa quadrangle records progressive deformation, as indicated by the temporal interleaving of stratigraphic units and structures. The deformation of both the long- and short-wavelength scales of the linear belts appears to be prolonged, deforming materials before, during, and after emplacement of regional plains.

REFERENCES CITED

Aubele, J.C., 1993, Venus small volcano classification and description, *in* Abstracts of papers submitted to the Twenty-fourth Lunar and Planetary Science Conference, part 1, Houston, March 15–19, 1993: Houston, Lunar and Planetary Institute, p. 47–48.

Baker, V.R., Komatsu, G., Parker, T.J., Gulick, V.C., Kargel, J.S., and Lewis, J.S., 1992, Channels and valleys on Venus: Preliminary analysis of Magellan data: Journal of Geophysical Research, v. 97, p. 13,421–13,444.

Banerdt, W.B., and Golombek, M.P., 1988, Deformational models of rifting and folding on Venus: Journal of Geophysical Research, v. 93, p. 4759–4772.

Banerdt, W.B., McGill, G.E., and Zuber, M., 1997, Plains tectonics on Venus: *in* Bougher, S.W., Hunten, D.M., and Phillips, R.J., eds., Venus II, Tucson, University of Arizona Press, p. 901–930.

Barsukov, V.L., and others, 1986, The geology and geomorphology of the Venus surface as revealed by the radar images obtained by Veneras 15 and 16, *in* Lunar and Planetary Science Conference, Sixteenth, Houston, March 11–15, 1985, Proceedings, part 2: Journal of Geophysical Research, v. 91, p. D378–D398.

Basilevsky, A.T., and Head, J.W., III, 1995, Global stratigraphy of Venus: Analysis of a random sample of thirty-six test areas: Earth, Moon, and Planets, v. 66, p. 285–336.

Basilevsky, A.T., Pronin, A.A., Ronca, L.B., Kryuchkov, V.P., Sukhanov, A.L., and Markov, M.S., 1986, Styles of tectonic deformations on Venus: Analysis of Venera 15 and 16 data, *in* Lunar and Planetary Science Conference, Sixteenth, Houston, March 11–15, 1985, Proceedings, part 2: Journal of Geophysical Research, v. 91, p. D399–D411.

Bilotti, F., Connors, C., and Suppe, J., 1993, Global organization of tectonic deformation of Venus, *in* Abstracts of papers submitted to the Twenty-fourth Lunar and Planetary Science Conference, part 1, Houston, March 15–19, 1993: Houston, Lunar and Planetary Institute, p. 107–108.

Bindschadler, D.L., Schubert, G., and Kaula, W.M., 1990, Mantle flow tectonics and the origin of Ishtar Terra, Venus: Geophysical Research Letters, v. 17, p. 1345–1348.

Campbell, B.A., 1995, Use and presentation of Magellan quantitative data in Venus mapping: U.S. Geological Survey Open File Report.

Campbell, D.B., Senske, D.A., Head, J.W., Hine, A.A., and Fisher, P.C., 1991, Venus southern hemisphere: Geologic character and age of terrains in the Themis-Alpha-Lada region: Science, v. 251, p. 180–183.

Campbell, D.B., Stacy, N.J.S., Newman, W.I., Arvidson, R.E., Jones, E.M., Musser, G.S., Roper, A.Y., and Schaller, C., 1992, Magellan observations of extended impact crater related features on the surface of Venus: Journal of Geophysical Research, v. 97, p. 16,249–16,277.

Chapman, M.G., 1999, Geologic map of the Galindo quadrangle (V–40), Venus: U.S. Geological Survey Geologic Investigations Series Map I–2613, 1:5,000,000 scale.

Farr, T.G., 1993, Radar interactions with geologic surfaces: Jet Propulsion Laboratory, Publication 93-24, p. 45–56.

Ford, J.P., Blom, R.G., Crisp, J.A., Elachi, C., Farr, T.G., Saunders, R.S., Theilig, E.E., Wall, S.D., and Yewell, S.B., 1989, Spaceborne radar observations: A guide for Magellan radar image analysis: Jet Propulsion Laboratory Publication 89-41, 126p.

Frank, S.L., and Head, J.W., 1990, Ridge belts on Venus: Morphology and origin: Earth, Moon, and Planets, v. 50/51, p. 421–470.

Gault, D.E., and Wedekind, J.A., 1978, Experimental studies of oblique impact, *in* Lunar and Planetary Science Conference, Ninth, Houston, March 13–17, 1978, Proceedings: Geochimica et Cosochimica Acta, v. 3, p. 3843–3875.

Grosfils, E.B., and Head, J.W., 1994, Emplacement of a radiating dike swarm in western Vinmara Planitia, Venus: Interpretation of the regional stress field orientation and subsurface magmatic configuration: Earth, Moon, and Planets, v. 66, p. 153–171.

Kryuchkov, V.P., 1988, Ridge belts on the plains of Venus, *in* Abstracts of papers submitted to the Nineteenth Lunar and Planetary Science Conference, part 2, Houston, March 14–18, 1988: Houston, Lunar and Planetary Institute, p. 649–650.

Lancaster, M.G., Guest, J.E., and Magee, K.P., 1995, Great lava flow fields on Venus: Icarus, v. 118, p. 69–86.

Masursky, H., Eliason, E., Ford, P.G., McGill, G.E., Pettengill, G.H., Schaber, G.G., and Schubert, G., 1980, Pioneer Venus radar results: Geology from images and altimetry: Journal of Geophysical Research, v. 85, p. 8232–8260.

Muhleman, D.O., 1964, Radar scattering from Venus and the Moon: Astronomical Journal, v. 69, p. 34–41.

Phillips, R.J., Grimm, R.E., and Malin, M.C., 1991, Hot-spot evolution and the global tectonics of Venus: Science, v. 252, p. 651–658.

Phillips, R.J., and Hansen, V.L., 1994, Tectonic and magmatic evolution of Venus: Annual Review of Earth and Planetary Science, v. 22, p. 597–654.

Schaber, G.G., Strom, R.G., Moore, H.J, Soderblom, L.A., Kirk, R.L., Chadwick, D.J., Dawson, D.D., and Gaddis, L.R., 1992, Geology and distribution of impact craters on Venus: What are they telling us?: Journal of Geophysical Research, v. 97, p. 13,257–13,301.

Schultz, P.H., 1992, Atmospheric effects on ejecta emplacement and crater formation on Venus from Magellan: Journal of Geophysical Research, v. 97, p. 16,183–16,248.

Senske, D.A., Campbell, D.B., Head, J.W., Fisher, P.C., Hine, A.A., deCharon, A., Frank, S.L., Keddie, S.T., Roberts, K.M., Stofan, E.R., Aubele, J.C., Crumpler, L.C., and Stacy, N., 1991, Geology and tectonics of the Themis Regio - Lavinia Planitia - Alpha Regio - Lada Terra area, Venus: Results from Arecibo image data: Earth, Moon, and Planets, v. 55, p. 97–161.

Solomon, S.C., Head, J.W., Kaula, W.M., McKenzie, D., Parsons, B., Phillips, R.J., Schubert, G., and Talwani, M., 1991, Venus tectonics: Initial analysis from Magellan: Science, v. 252, p. 297–312.

Solomon, S.C., Smrekar, S.E., Bindschadler, D.L., Grimm, R.E., Kaula, W.M., McGill, G.E., Phillips, R.J., Saunders, R.S., Schubert, G., Squyres, S.W., and Stofan, E.R., 1992, Venus tectonics: An overview of Magellan observations: Journal of Geophysical Research, v. 97, p. 13,199–13,255.

Squyres, S.W., Janes, D.M., Schubert, G., Bindschadler, D.L., Moersch, J.E., Turcotte, D.L., and Stofan, E.R., 1993, The spatial distribution of coronae and related features on Venus: Geophysical Research Letters, v. 20, p. 2965–2968.

Squyres, S.W., Jankowski, D.G., Simons, M., Solomon, S.C., Hager, B.H., and McGill, G.E., 1992, Plains tectonism on Venus: The deformation belts of Lavinia Planitia: Journal of Geophysical Research, v. 97, p. 13,579–13,599.

Stofan, E.R., Sharpton, V.L., Schubert, G., Baer, G., Bindschadler, D.L., Janes, D.M., and Squyres, S.W., 1992, Global distribution and characteristics of coronae and related features on Venus: Implications for origin and relation to mantle processes: Journal of Geophysical Research, v. 97, p. 13,347–13,378.

Strom, R.G., Schaber, G.G., and Dawson, D.D., 1994, The global resurfacing of Venus: Journal of Geophysical Research, v. 99, p. 10,899–10,926.

Sukhanov, A.L., and Pronin, A.A., 1989, Ridged belts on Venus as extensional features: *in* Lunar and Planetary Science Conference, Nineteenth, Houston, March 14–18, 1989, Proceedings: Houston, Lunar and Planetary Institute, p. 335–348.

Sukhanov A.L., Pronin, A.A., Burba, G.A., Nikishin, A.M., Kryuchkov, V.P., Basilevsky, A.T., Markov, M.S., Kuzmin, R.O., Bobina, N.N., Shashkina, V.P., Slyuta, E.N., and Chernaya, I.M., 1989, Geomorphic/geologic map of part of the northern hemisphere of Venus: U.S. Geological Survey Miscellaneous Investigations Series Map I–2059, scale 1:15,000,000.

Zimbelman, J.R., 1995, Preliminary mapping of the Bellona Fossae (V–15) quadrangle on Venus: Geological Society of America Abstracts with Programs, v.27, p. 208.

Zuber, M.T., 1987, Constraints on the lithospheric structure of Venus from mechanical models and tectonic surface features: Journal of Geophysical Research, v. 92, p. E541–E551.

Zuber, M.T., 1990, Ridge belts: Evidence for regional- and large-scale deformation on the surface of Venus: Geophysical Research Letters, v. 17, p. 1369–1372.

Zuber, M.T., and Parmentier, E.M., 1990, On the relationship between isostatic elevation and the wavelengths of tectonic surface features on Venus: Icarus, v. 85, p. 290–308.

TABLE 1. *Physical properties of mapped units.*

[Symbols of units listed in this table are the same symbols used on the geologic map. At least one sample was taken for each unit. Regionally widespread units (pr_a, pr_b, pr_c, and t) and some local units (fd and flb) that outcrop over a large enough range of latitudes for the incidence angle to change significantly were sampled in two or three places. In these cases, sample numbers are indicated. Table displays information on sample locality, pixel scale (Δ), number of pixels used in calculating backscatter (N), incidence angle (ι, angle between SAR beam and a normal to an assumed spherical surface where beam hits), radius, normalized backscatter cross section (σ_o), root mean square slope (θrms) for meter and larger scale slopes, Fresnel reflectivity (ρ), emissivity, and dielectric constants calculated for smooth-surface (εs) and rough surface (εr) cases. For σ_o, values in parentheses represent ±1 standard deviation about the mean. For all other data, numbers in parentheses represent minimum and maximum values of each parameter within confines of chosen sample boundaries. All mapped units are represented in these tables with one exception: linear belt material c is not represented because its material type is unresolved. Sizes of sample boxes represent maximum size admissible to accurately represent unit; for instance, sample box for a unit that contains a dense population of radar-bright structures must be small enough to fit between structures, which are not inherent properties of the material. Sample box for a widespread regional material, however, may be much larger because it is possible to define a larger area without any structural interferences or presence of other material units.]

Unit		Latitude; Longitude	Δ (m)	N	ι	Radius (km)
t	1	56.980–57.530 N; 201.230–202.020 E	225	45232	29	6051.387 (6049.708, 6052.135)
	2	59.430–60.690 N; 229.390–231.160 E	225	217175	28	6051.229 (6050.416, 6051.691)
pr_c	1	51.740–52.540 N; 232.330–233.480 E	225	105183	32	6051.378 (6051.254, 6051.629)
	2	62.550–63.180 N; 209.730–212.880 E	225	181621	27	6051.229 (6050.892, 6051.417)
pr_b	1	69.920–70.720 N; 223.260–226.040 E	225	254562	24	6051.535 (6051.440, 6051.670)
	2	72.120–73.450 N; 182.640–187.100 E	225	130788	23	6051.743 (6051.447, 6051.896)
pr_a	1	53.360–54.420 N; 200.630–203.690 E	225	404000	31	6051.473 (6051.290, 6051.780)
	2	58.830–60.950 N; 182.770–184.860 E	225	440674	28	6050.960 (6050.729, 6050.993)
	3	67.300–68.830 N; 209.450–212.890 E	225	418458	25	6050.973 (6050.758, 6051.174)
pm		55.940–56.610 N; 212.020–214.330 E	225	183226	30	6051.986 (6051.742, 6052.230)
pt		65.060–65.140 N; 225.840–226.110 E	225	1591	26	6051.208 (6051.134, 6051.395)
bl_a		48.360–48.730 N; 218.380–218.550 E	225	7875	33	6051.742 (6051.695, 6051.847)
bl_b		55.950–56.080 N; 208.390–208.610 E	225	3564	30	6052.175 (6051.737, 6052.305)
ld		56.960–57.160 N; 200.500–200.890 E	225	8448	29	6051.107 (6050.180, 6051.607)
ps		55.620–55.730 N; 207.710–207.780 E	225	1071	30	6052.392 (6052.372, 6052.405)
fd	1	55.390–56.050 N; 218.280–219.370 E	225	75746	30	6051.901 (6051.816, 6052.177)
	2	72.020–72.300 N; 199.250–200.340 E	225	18221	23	6051.394 (6050.987, 6051.545)
fs		70.530–70.860 N; 198.170–199.050 E	225	17538	24	6050.767 (6050.339, 6051.125)
flb	1	48.580–48.850 N; 212.080–212.560 E	225	17024	33	6051.026 (6050.450, 6051.197)
	2	48.900–49.400 N; 213.980–214.880 E	225	56165	29	6051.107 (6050.180, 6051.607)
c		60.070–60.570 N; 223.570–224.710 E	225	10400	28	6051.132 (6051.003, 6051.294)
cf		60.070–60.570 N; 223.570–224.710 E	225	49533	28	6051.132 (6051.003, 6051.294)
co_a		64.990–65.090 N; 208.200–208.460 E	225	2548	26	6051.300 (6050.396, 6051.403)
co_b		64.130–64.760 N; 208.290–209.260 E	225	57424	26	6050.948 (6050.795, 6051.011)
co_c		65.050–65.230 N; 205.950–206.330 E	225	5994	26	6050.655 (6050.265, 6050.912)
flt		72.910–73.060 N; 238.330–238.830 E	225	3692	23	6051.232 (6051.159, 6051.287)

Unit		σ_o (dB)	θrms (deg)	ρ	Emissivity	εs, εr
t	1	–7.621 (–12.952, –5.299)	5.95 (2.90, 10.40)	0.089 (0.045, 0.170)	0.906 (0.896, 0.914)	3.0, 3.5
	2	–7.393 (–14.532, –4.824)	4.57 (1.20, 10.40)	0.070 (0.045, 0.175)	0.902 (0.888, 0.909)	3.1, 3.6
pr_c	1	–14.791 (–16.359, –13.641)	2.16 (0.70, 4.10)	0.127 (0.080, 0.160)	0.859 (0.850, 0.873)	3.8, 4.8
	2	–12.432 (–14.253, –11.153)	2.47 (0.90, 5.10)	0.115 (0.075, 0.175)	0.868 (0.861, 0.877)	3.9, 4.6
pr_b	1	–12.389 (–13.774, –11.341)	2.36 (1.40, 2.90)	0.125 (0.105, 0.150)	0.857 (0.853, 0.860)	4.3, 4.9
	2	–11.723 (–13.214, –10.615)	1.54 (0.60, 2.60)	0.108 (0.075, 0.130)	0.857 (0.854, 0.860)	4.3, 4.9
pr_a	1	–12.122 (–13.424, –11.105)	3.12 (1.50, 4.60)	0.130 (0.085, 0.185)	0.872 (0.862, 0.884)	3.6, 4.4
	2	–11.917 (–13.427, –10.798)	2.67 (1.40, 4.30)	0.126 (0.105, 0.155)	0.867 (0.859, 0.877)	3.8, 4.6
	3	–10.799 (–12.279, –9.697)	2.89 (1.80, 4.20)	0.100 (0.065, 0.130)	0.874 (0.867, 0.881)	3.8, 4.4
pm		–11.715 (–14.545, –10.017)	1.69 (0.80, 3.20)	0.140 (0.105, 0.175)	0.849 (0.838, 0.869)	4.1, 5.1
pt		–8.205 (–10.941, –6.540)	6.06 (5.50, 7.20)	0.097 (0.080, 0.110)	0.890 (0.890, 0.891)	3.4, 3.9
bl_a		–9.971 (–12.594, –8.347)	2.38 (1.90, 3.10)	0.095 (0.085, 0.105)	0.889 (0.887, 0.892)	3.1, 3.9
bl_b		–7.050 (–12.718, –4.672)	3.45 (2.40, 6.00)	0.113 (0.100, 0.140)	0.892 (0.890, 0.894)	3.2, 3.9
ld		–9.208 (–12.142, –7.473)	3.04 (2.20, 3.60)	0.070 (0.055, 0.075)	0.896 (0.895, 0.899)	3.1, 3.8
ps		–11.499 (–12.897, –10.443)	2.48 (1.80, 2.90)	0.096 (0.090, 0.100)	0.870 (0.870, 0.871)	3.7, 4.5
fd	1	–10.129 (–14.426, –8.012)	2.44 (1.30, 3.70)	0.120 (0.095, 0.145)	0.863 (0.856, 0.868)	3.8, 4.7
	2	–7.888 (–9.187, –6.890)	4.20 (1.50, 7.50)	0.084 (0.070, 0.135)	0.887 (0.881, 0.891)	3.6, 4.0
fs		–7.244 (–12.041, –5.020)	4.66 (2.30, 7.30)	0.102 (0.075, 0.170)	0.894 (0.892, 0.895)	3.4, 3.9
flb	1	–6.971 (–8.265, –5.976)	4.46 (2.90, 6.50)	0.119 (0.095, 0.155)	0.889 (0.881, 0.892)	3.1, 3.9
	2	–12.281 (–14.325, –10.897)	2.50 (1.00, 4.10)	0.126 (0.100, 0.160)	0.859 (0.847, 0.865)	3.7, 4.8
c		–7.198 (–9.589, –5.665)	2.26 (1.00, 3.90)	0.081 (0.045, 0.125)	0.895 (0.884, 0.906)	3.2, 3.8
cf		–11.557 (–14.218, –9.920)	2.26 (1.00, 3.90)	0.081 (0.045, 0.125)	0.895 (0.884, 0.906)	3.2, 3.8
co_a		–9.467 (–10.799, –8.449)	5.03 (2.10, 6.10)	0.113 (0.070, 0.135)	0.891 (0.888, 0.892)	3.4, 3.9
co_b		–11.803 (–13.319, –10.681)	2.62 (2.00, 4.10)	0.106 (0.080, 0.130)	0.876 (0.870, 0.882)	3.7, 4.3
co_c		–6.757 (–10.182, –4.866)	6.08 (5.20, 10.30)	0.117 (0.090, 0.220)	0.892 (0.890, 0.895)	3.4, 3.9
flt		–5.525 (–14.432, -2.804)	1.74 (1.40, 2.50)	0.102 (0.100, 0.110)	0.859 (0.858, 0.860)	4.3, 4.8

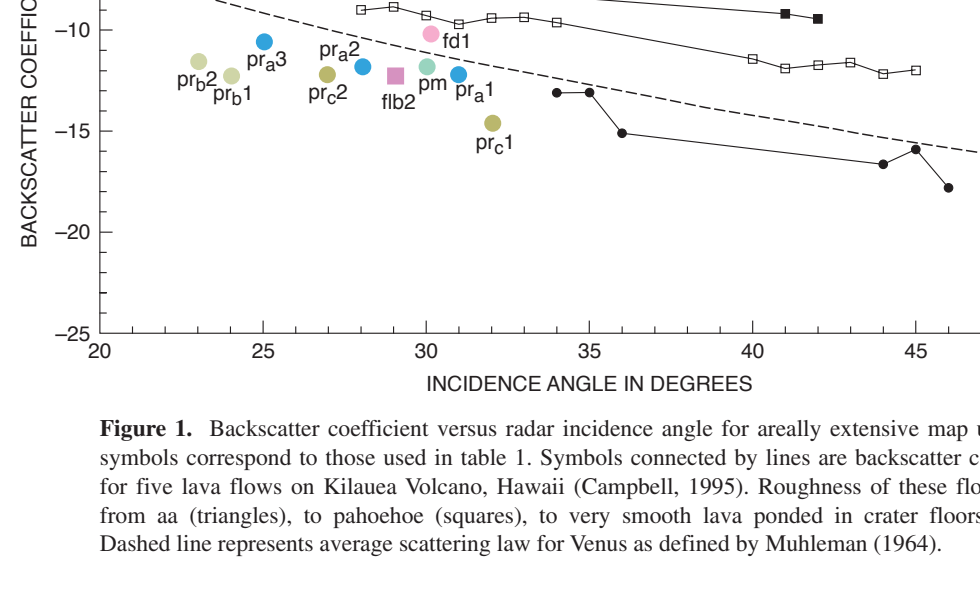

Figure 1. Backscatter coefficient versus radar incidence angle for areally extensive map units. Unit symbols correspond to those used in table 1. Symbols connected by lines are backscatter coefficients for five lava flows on Kilauea Volcano, Hawaii (Campbell, 1995). Roughness of these flows ranges from aa (triangles), to pahoehoe (squares), to very smooth lava ponded in crater floors (circles). Dashed line represents average scattering law for Venus as defined by Muhleman (1964).

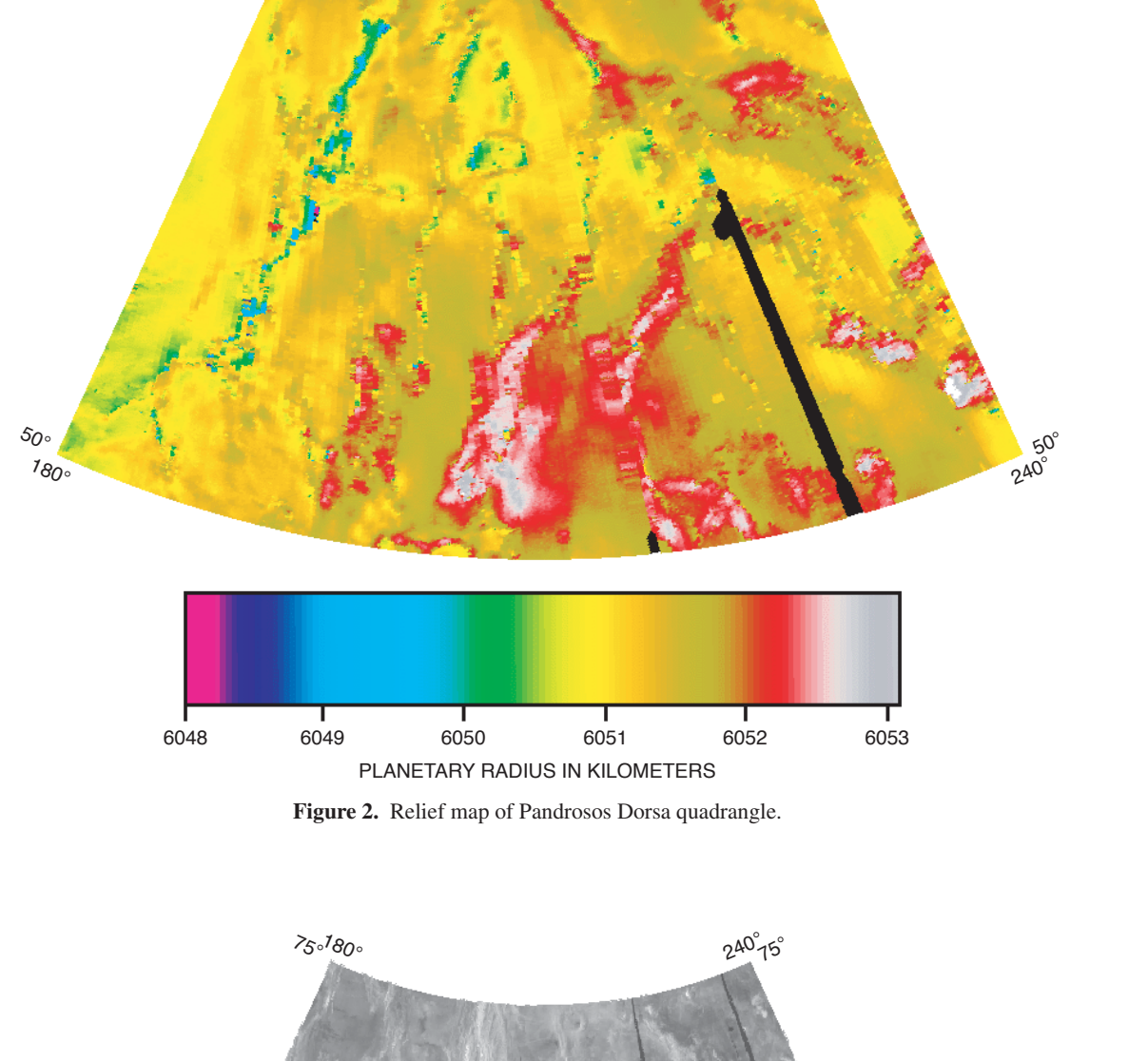

Figure 2. Relief map of Pandrosos Dorsa quadrangle.

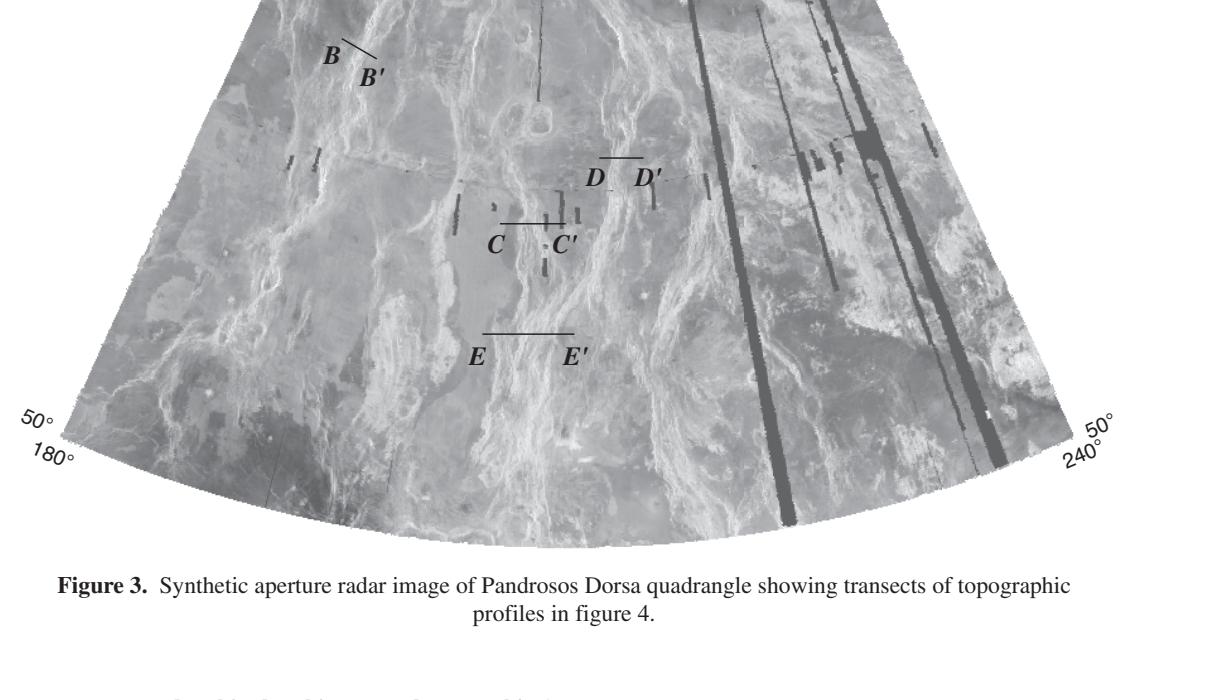

Figure 3. Synthetic aperture radar image of Pandrosos Dorsa quadrangle showing transects of topographic profiles in figure 4.

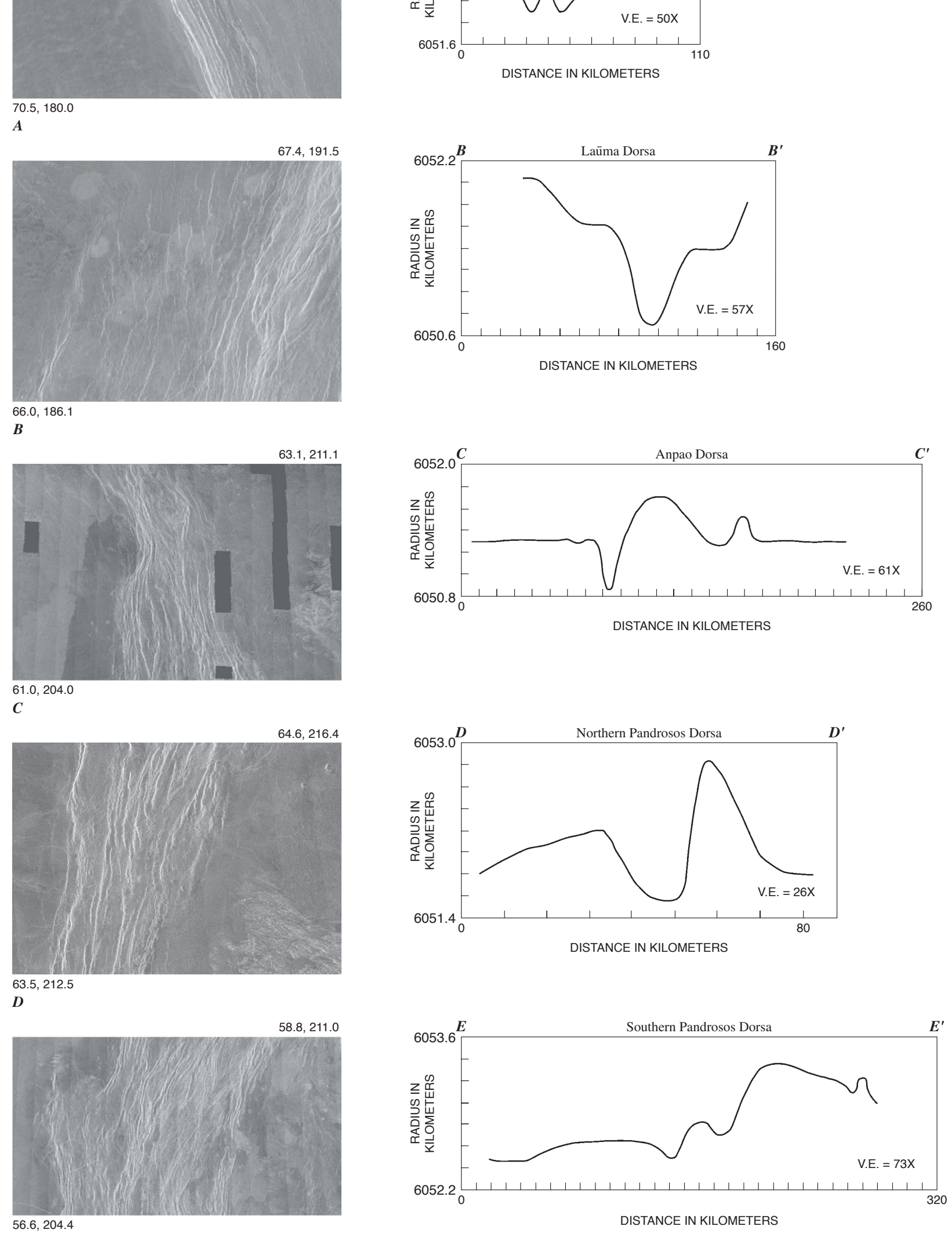

Figure 4. Full resolution synthetic aperture radar images and topographic profiles across major linear belts (fig. 3). ***A***, Lukelong Dorsa; ***B***, Laūma Dorsa; ***C***, Anpao Dorsa; ***D***, northern Pandrosos Dorsa; ***E***, southern Pandrosos Dorsa.

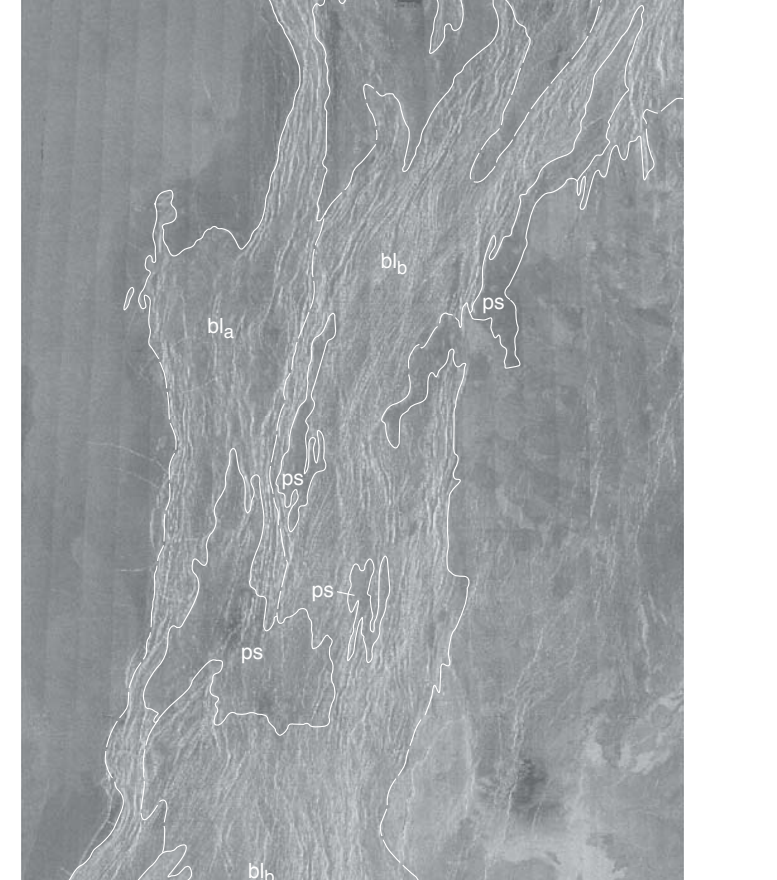

Figure 5. Geologic sketch map of southern Pandrosos Dorsa. [illegible] of smooth plains material (unit ps) in center of belt contains dozens of small shields and domes, which defines region as a shield field. bl_a, bl_b: Linear belt materials a and b, respectively.

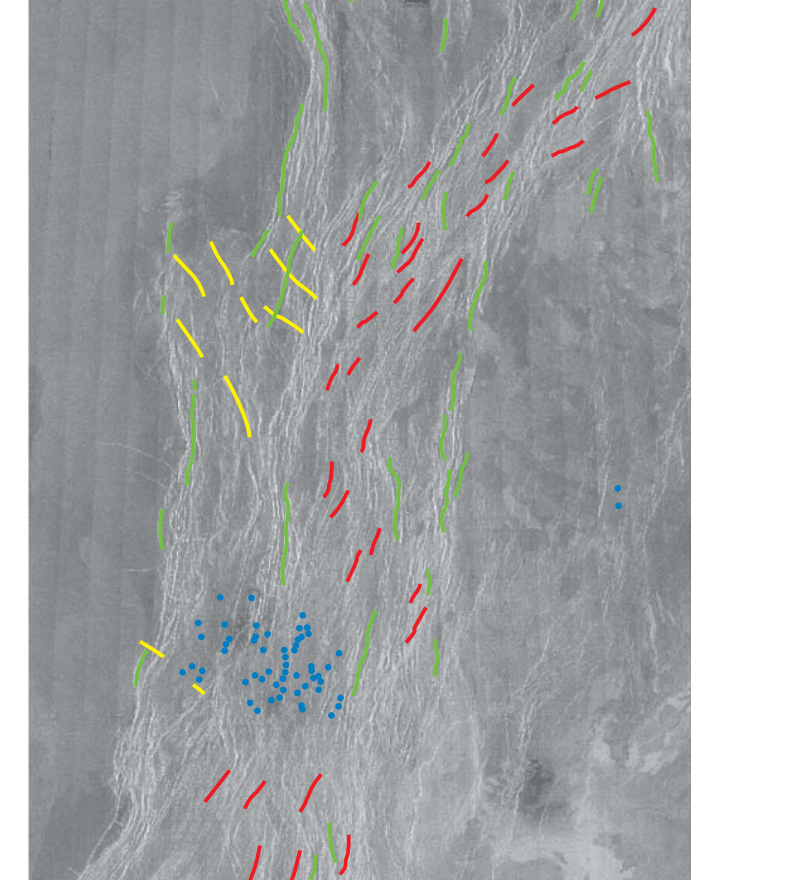

Figure 6. Structural features within southern Pandrosos Dorsa. Sche[illegible] by red lines. Note the generally parallel north south trend of both types of structures. Younger linear features trending northwest-southeast are shown in yellow; volcanic shields and domes are shown as blue dots.

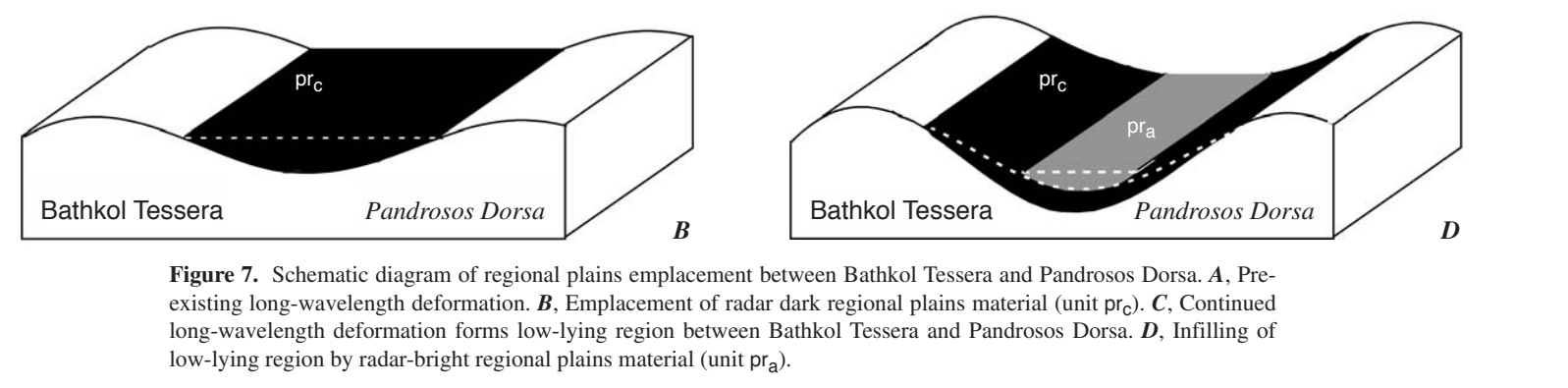

Figure 7. Schematic diagram of regional plains emplacement between Bathkol Tessera and Pandrosos Dorsa. ***A***, Preexisting long-wavelength deformation. ***B***, Emplacement of radar dark regional plains material (unit pr_c). ***C***, Continued long-wavelength deformation forms low-lying region between Bathkol Tessera and Pandrosos Dorsa. ***D***, Infilling of low-lying region by radar-bright regional plains material (unit pr_a).

GEOLOGIC MAP OF THE PANDROSOS DORSA QUADRANGLE (V–5), VENUS

By

Elizabeth Rosenberg and George E. McGill

2001

ISBN 0-607-96392-1
9 780607 963922

For sale by U.S. Geological Survey, Information Services, Box 25286, Federal Center, Denver, CO 80225, 1–888–ASK–USGS

Printed on recycled paper